WADC TECHNICAL REPORT 54-113
PART I

THREE-DIMENSIONAL SUPERSONIC FLUTTER MODEL TESTS NEAR MACH NUMBER 1.5

Part 1. Model Design and Testing Techniques

JOHN F. McCARTHY, JR.
GIFFORD W. ASHER
JOHN S. PRIGGE, JR.
GILBERT M. LEVEY

MASSACHUSETTS INSTITUTE OF TECHNOLOGY

DECEMBER 1955

AIRCRAFT LABORATORY
CONTRACT AF 33(038)-22955
PROJECT 1370-13474

WRIGHT AIR DEVELOPMENT CENTER
AIR RESEARCH AND DEVELOPMENT COMMAND
UNITED STATES AIR FORCE
WRIGHT-PATTERSON AIR FORCE BASE, OHIO

Carpenter Litho & Prtg. Co., Springfield, O.
100 - July 1956

FOREWORD

This report, which describes the techniques of flutter model testing, was prepared by the Aeroelastic and Structures Research Laboratory, Massachusetts Institute of Technology. The work was performed under the direction of Professor R.L. Halfman, and the project was supervised by Mr. John F. McCarthy, Jr. The work was accomplished on Air Force Contract No. AF33(038)-22955, under Project 1370-13474 "Three-Dimensional Supersonic Flutter Model Tests at Mach Number 1.5." This project was initiated and administered by the Dynamics Branch of the Aircraft Laboratory, Directorate of Laboratories, Wright Air Development Center, with Mr. W. J. Mykytow and Mr. N. R. Hoffman acting as project engineers. This report is the second in a series of reports that will be issued covering the work done under this contract.

The authors are indebted to Mr. G. M. Falla for the photography, and to Messrs. J. R. Friery and G. Anitole for help in preparing the figures.

ABSTRACT

The design and construction of a series of supersonic flutter models are described. The techniques of static, vibration, and flutter testing are discussed. Some recommendations for future model design and testing are presented, and evaluation of the present methods is made. The accuracy of the various measurements is discussed.

PUBLICATION REVIEW

This report has been reviewed and is approved

FOR THE COMMANDER

E H Schwartz

For D. D. McKEE
Colonel, USAF
Chief, Aircraft Laboratory

TABLE OF CONTENTS

LIST OF ILLUSTRATIONS

LIST OF SYMBOLS

a	distance aft of leading edge of a structural element
b	semichord of a surface
B	spar width
C	dimensionless constant for model frequency equations
(cg)	section center of gravity position aft of the leading edge
(ea)	position of elastic axis aft of the leading edge
f	frequency (cycles per second)
g	coefficient of structural damping
EI	bending flexural rigidity
GJ	torsional rigidity
H	spar height
H_T	tunnel test section height
k	spring constant or stiffness influence coefficient
L	semispan of a surface
m	mass per unit span of a surface
M	total mass
MN	Mach number
N	number of cycles to damp to half amplitude
p	static pressure
p_o	stagnation pressure
q_i	generalized coordinate of motion
r_α	nondimensional radius of gyration of a section about the elastic axis based on semichord
T	static temperature
T_o	stagnation temperature
y	spanwise length coordinate
α	angle of attack
β	nondimensional constant for Eq. (2.8)
$\sum_i$	sum over i elements
λ	taper ratio (ratio of tip to root chord)

ρ	air density
ρ_o	stagnation density
μ	relative wing density $\rho = m/\pi\rho\ b^2$
ω	circular frequency

SUBSCRIPTS

o	value of a parameter at the root chord
α	refers to torsional motions
h	refers to bending motions
1, 2, 3. . .	first, second, third . . . modes

A bar superscript indicates that a quantity is taken with reference to the elastic axis.

SECTION I

INTRODUCTION

Section II of this report discusses the design, construction, and testing of a series of supersonic flutter models. It is not the intention of this report to present in great detail the methods and techniques used in this flutter program. The purpose will be to discuss briefly those techniques of measurement and testing that were successful, and hence were used in obtaining the flutter data. It is felt that this sort of information may be useful for future programs in supersonic flutter testing.

When this program of supersonic flutter testing was initiated, there was little previous experience in supersonic flutter testing in wind tunnels upon which to draw. Most previous experience had been gained on either rocket propelled models or on solid metal models of high density. Little work had been done on wind tunnel models of low density in the supersonic range above Mach numbers of 1.3.

The first step in the present program was the design, construction, and calibration of a supersonic flutter facility. Reference 9 describes the continuously variable Mach number blow-down tunnel that was used to obtain the flutter data of this program. The tunnel has proved admirably suited to flutter testing because a flutter boundary may be found by varying flow parameters rather than model parameters. Flow deviations in the test section are small over the entire Mach number range of the tunnel of 1.3 to 2.1.

Section 2.1 describes the design and construction of the supersonic flutter models tested in this program. They are simple in construction and hence are inexpensive to build.

The design of lightweight supersonic flutter models presents some difficulties. Because the models are generally destroyed if supersonic flutter occurs, the models should be inexpensive to build. The small size of the models generally required can also be a problem when efficient structural elements are required in the model for lightweight. In spite of the high dynamic pressures encountered in supersonic flutter testing, the static strength of the

Manuscript released by the authors December 1955 for publication as a WADC Technical Report.

models is generally adequate. The models are stiff because of the requirement that the Mach number of the model must equal the full scale Mach number. Reference 1 shows that this requirement results in a model of high stiffness and frequency because of the small size. No difficulty in static strength of the models was encountered during the present program. However, supersonic flutter models of light weight are generally not strong enough to withstand the starting shock associated with the establishment of supersonic flow in the tunnel test section. It appears important to either restrain the model during the start of a run or to inject the model into the test section after supersonic flow is established. The latter alternative was chosen for this program. The mechanism for injecting models is described in Reference 9. No problems arise provided the model is injected into a regime of the flow in which it is stable. The model can then be brought to an unstable region by changing the flow parameters. Models will flutter on injection if an attempt is made to inject the model into a flow regime in which it is unstable. Some buffeting occurs on injection, but for the models tested in this program it was not serious. For models with control surfaces of low natural frequency, injection could cause some difficulties.

The static and vibration testing techniques are described in Sections 2.2 and 2.3. No major difficulties were encountered in obtaining reliable vibration data. To obtain flexibility influence coefficients to the desired accuracy with a reasonable amount of labor, deflection measurements were made using linear variable differential transformers, or Schaevitz coils. This system is described in Section 2.2. Otherwise static tests followed traditional lines.

The continuous variation of flow parameters possible in the supersonic blow-down tunnel has proved very successful for flutter testing since it eliminates the need for either a number of different test runs or a number of models of varying parameters to find a flutter point. As noted in Section 2.4, the present tunnel operates at a constant stagnation pressure. Therefore, the density varies during a single run with Mach number, but by controlling stagnation pressure such density variations could be eliminated. The use of an intermittent type tunnel has been no problem, but means only that instrumentation must be carefully checked before each run in order that the run shall not be aborted. In the present program the model instrumentation was simple and only a few runs were aborted due to faulty instrumentation. The variation in Mach number is relatively slow – about 100 chord lengths of flow pass over the model per 0.01 Mach number change – so that the flow is quasi-steady. No difficulties arise from the continuous variation in Mach number during a flutter run.

SECTION II

MODEL DESIGN AND TESTING TECHNIQUES

2.1 Model Design and Construction

Models were constructed for three basic planforms – straight, swept, and delta. These are shown in Fig. 1. The design and construction of all these planforms were basically the same. An aluminum spar was used to give the required stiffness and stiffness distribution. Lead weights were used to control the mass distribution. Balsa wood, cemented to the spar was used to give the proper aerodynamic shape. The general layout of these elements of the wing is shown in Fig. 2. They are also seen in Fig. 3, which shows a swept wing and a straight wing with aileron under construction. A finished straight wing with an attached tip tank is shown in Fig. 4.

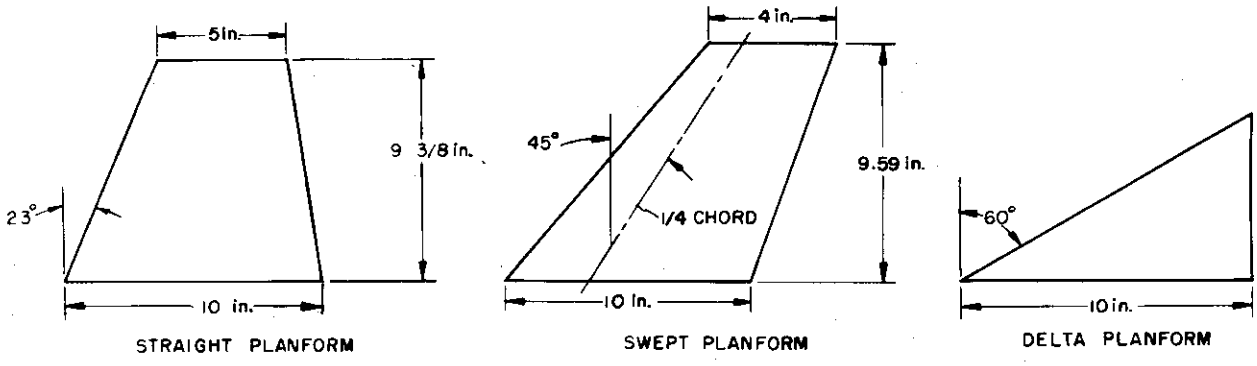

Fig. 1. Basic wing planforms.

All of the wings were designed using the concept of a straight locus of shear centers, an elastic axis. Stiffness distributions were described by specifying the distribution of EI, bending flexural rigidity, and GJ, torsional rigidity, along the elastic axis. This means essentially that chordwise deformations of the structure were considered to be small. The assumption of small chordwise deformations seems justified, even for the delta wing models, in the light of the flexibility influence coefficient data and vibration mode shape data that was obtained. For straight and delta wings the influence coefficient data presented in Reference 2 shows that there is little chordwise bending and the vibration data of Reference 2 shows that the first three vibration modes

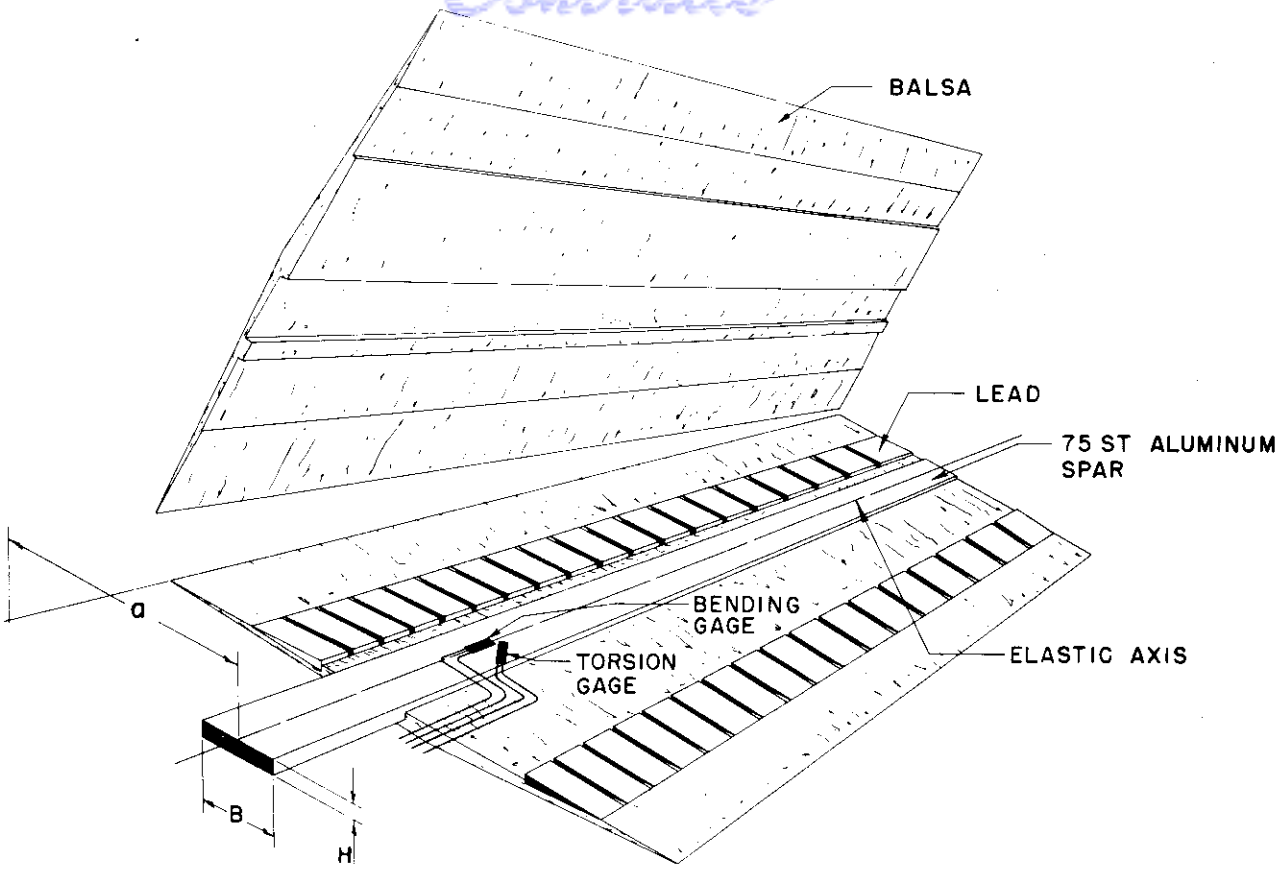

Fig. 2. Exploded view of straight wing.

have shapes that are free from significant chordwise deformations. Figure 16 shows nodal lines for the first four vibration modes of a swept wing. Significant chordwise deformations are absent. Therefore, the use of the elastic axis concept for the model wings of this program seems justified. The absence of significant chordwise deformations also simplifies the problem of specifying the mass properties of the models, since it then becomes necessary only to specify the mass per unit span, the radius of gyration of a section about the elastic axis, and the chordwise center of gravity of a section. Detailed chordwise mass distribution is arbitrary as long as the aforementioned properties are maintained, making it possible to control the wing mass properties by the simple system of two concentrated lead weights fore and aft of the spar as shown in Figs. 2 and 3.

The mass and stiffness properties of the model wings designed for this program were simple. Both torsional and bending stiffness were varied as the fourth power of the chord or:

$$\overline{EI} = \overline{EI}_o \left[1 - (1 - \lambda)\, \overline{y}/\overline{L}\right]^4 \qquad (2.1)$$

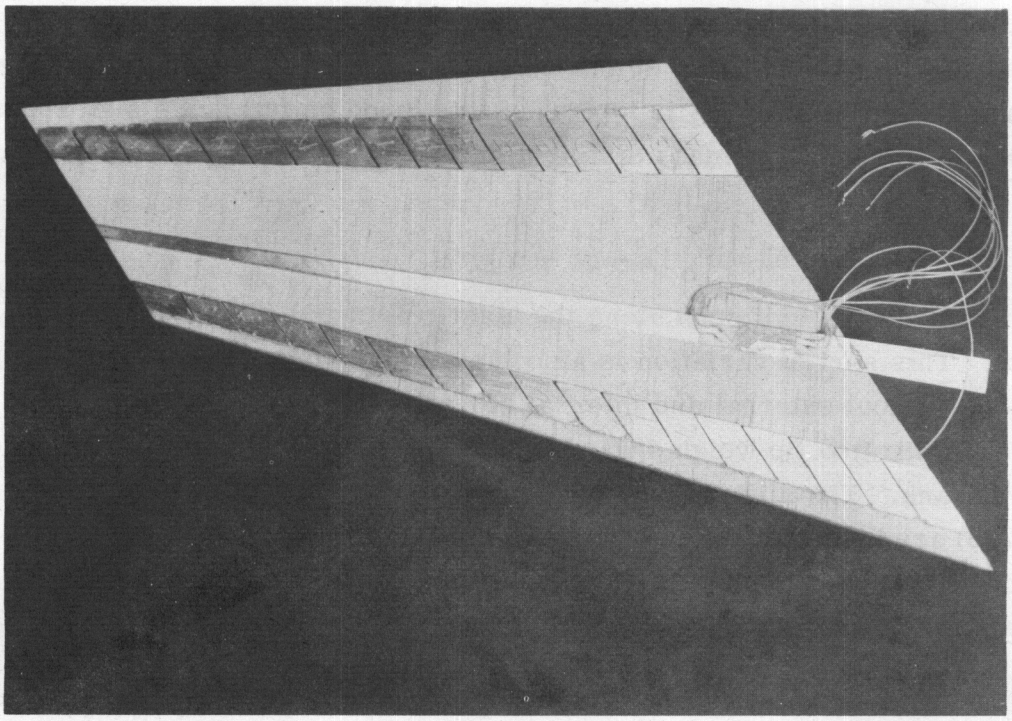

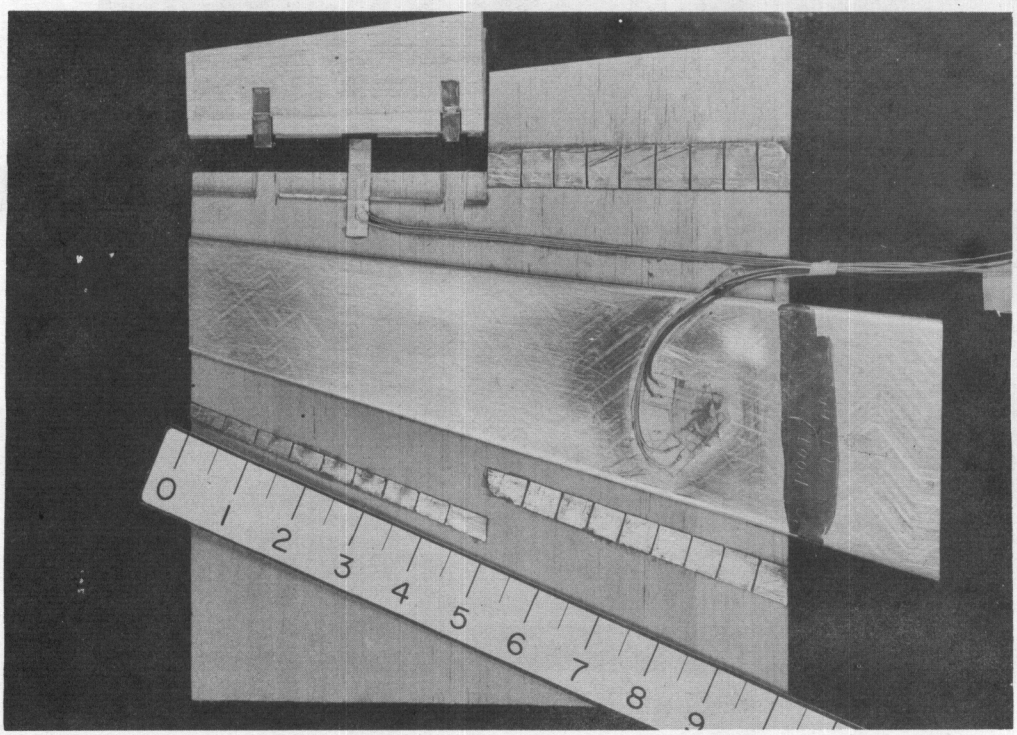

Fig. 3. Straight and swept wings under construction.

$$\overline{GJ} = \overline{GJ}_o [1 - (1 - \lambda)\bar{y}/\bar{L}]^4 \qquad (2.2)$$

where λ is the ratio of tip chord to root chord, $\bar{y}$ is the spanwise coordinate along the elastic axis, and $\bar{L}$ is the semispan of the wing along the elastic axis. This smooth variation in stiffness is typical of that found on full scale high speed aircraft lifting surfaces. The mass distribution was varied as the second power of the chord or:

$$\overline{m} = \overline{m}_o [1 - (1 - \lambda)\bar{y}/\bar{L}]^2 \qquad (2.3)$$

where $\overline{m}$ is the mass per unit span along the elastic axis and $\overline{m}_o$ the value of $\overline{m}$ at the root. This sort of variation is also typical of that found on real aircraft lifting surfaces without external and internal stores. For some models the presence of concentrated tip weights was simulated. Figure 4 shows a straight wing with a tip tank. The stiffness and mass distributions given by Eqs. (2.1), (2.2), and (2.3) are also convenient for the construction used in the models of this program, since solid elements which have linearly tapering cross sections have stiffness and mass distributions given by these equations. For the models

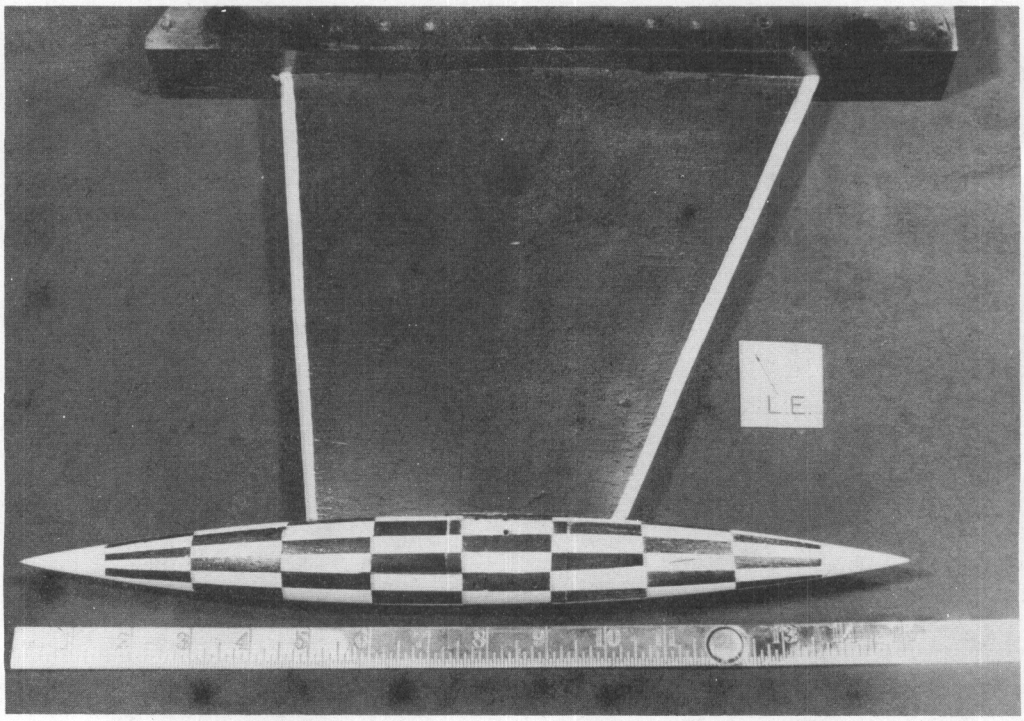

Fig. 4. Finished straight wing with tip tank.

of this program, chordwise center of gravity location, radius of gyration about the elastic axis, and elastic axis position were all held constant along the span.

In any specific wing design, spar size was determined from the first torsion and first bending frequency requirements. Generally, a certain level of first torsional frequency was required and the ratio of first bending to first torsional frequency for a given model was fixed. With the assumption of an elastic axis these frequencies are given by:

$$\omega_{\alpha 1} = \frac{C_{\alpha 1}}{\bar{L}} \sqrt{\frac{\overline{GJ}_o}{\bar{r}_\alpha^2 \, \bar{b}_o^2 \, \bar{m}_o}} \tag{2.4}$$

and

$$\omega_{h1} = \frac{C_{h1}}{\bar{L}^2} \sqrt{\frac{\overline{EI}_o}{\bar{m}_o}} \tag{2.5}$$

where ω_{h1} and $\omega_{\alpha 1}$ are the required frequencies, $\bar{r}_\alpha$ is the nondimensional radius of gyration, and C_{h1} and $C_{\alpha 1}$ are nondimensional constants which depend on model mass and stiffness distribution. The constants C_{h1} and $C_{\alpha 1}$ can be determined experimentally, may be calculated theoretically, or may be found in handbooks such as Reference 3 for simple distributions of mass and stiffness. Equations (2.4) and (2.5) have been found very useful for the design of the models used in this program. First torsional and first bending frequencies can be predicted within about ±5% with the use of Eqs. (2.4) and (2.5).

An equation similar to Eqs. (2.4) and (2.5) can be written for the second bending frequency, but its application to the models of this program has not been too successful since the spread between predicted and measured frequencies is larger than it is for first and second torsion frequencies. This fact is unfortunate since small changes in second bending to first torsion frequency ratio may have large effects on the flutter speed if the ratio is near unity. It would, of course, be desirable to have accurate control over second bending for design purposes. The problem of control over second bending becomes especially acute when the simulation of a specific airplane configuration is desired.

If $\omega_{\alpha 1}$ is specified and the wing mass parameters are known, then Eq. (2.4) gives the required total $\overline{GJ}_o$ of the model. The required ratio of ω_{h1} to $\omega_{\alpha 1}$ fixes the ratio of $\overline{EI}_o$ to $\overline{GJ}_o$ since $\omega_{h1}/\omega_{\alpha 1}$ can be written:

$$\omega_{h1}/\omega_{\alpha 1} = K \sqrt{\frac{\overline{EI}_o}{\overline{GJ}_o}} \tag{2.6}$$

for a wing whose mass and stiffness distribution, and geometry have been fixed. K is a constant depending, of course, on the geometry of the model and C_{h1} and $C_{\alpha 1}$. With the required $\overline{EI}_o$ and $\overline{GJ}_o$ for the wing known from application of Eqs. (2.4) and (2.6), the required $\overline{EI}_{ospar}$ and $\overline{GJ}_{ospar}$ can be found by subtracting from the total $\overline{EI}_o$ and $\overline{GJ}_o$ the values of $\overline{EI}_o$ and $\overline{GJ}_o$ for the balsa wood coverings. Lead weights are slit in a chordwise direction to minimize their contribution to the stiffness. For the models of this program the lead weights were assumed to contribute no stiffness, an assumption that was quite well borne out by static and vibration tests. For a solid rectangular spar $\overline{EI}_{ospar}$ and $\overline{GJ}_{ospar}$ are given by:

$$\overline{EI}_{ospar} = \frac{1}{12} \bar{B}_o \bar{H}_o^3 E \qquad (2.7)$$

and

$$\overline{GJ}_{ospar} = \beta (\bar{B}_o/\bar{H}_o) \bar{B}_o \bar{H}_o^3 G \qquad (2.8)$$

where $\bar{B}_o$ and $\bar{H}_o$ are the spar root width and height, and $\beta (\bar{B}_o/\bar{H}_o)$ is a constant depending on the ratio of width to depth of the spar. Values of β may be found in a number of texts such as References 1 and 4. A curve of β is shown in Fig. 5. Since the ratio of E to G for most structural materials is the same,

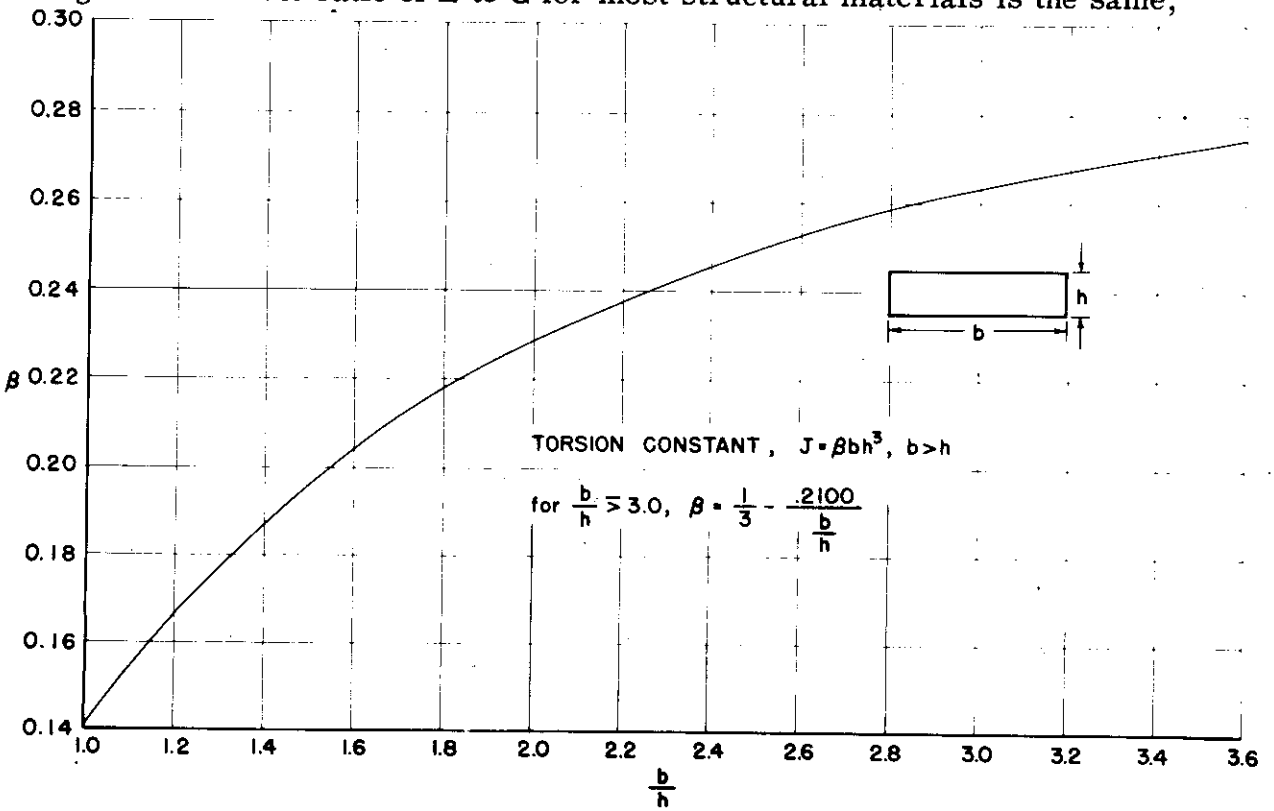

Fig. 5. Values of β for torsion constant of solid rectangular cross section.

inspection of Eqs. (2.7) and (2.8) shows that the ratio of $\overline{EI}_{ospar}$ to $\overline{GJ}_{ospar}$ and hence wing $\omega_{h1}/\omega_{\alpha 1}$ is determined by β once the mass, stiffness, and geometry of the wing have been fixed. The constant β is a function of the ratio $\overline{B}_o/\overline{H}_o$, and so the ratio of spar width to height is determined by the desired ratio of $\omega_{h1}/\omega_{\alpha 1}$. The over-all size of the spar is determined by the level of $\overline{GJ}_{ospar}$ required to give the torsional frequency.

Once the spar size and shape has been determined its position can be determined from the required elastic axis or shear center position. Reference 1 shows that, with the definition of elastic axis or shear center used for the design of the models of this report, the shear center lies at the centroid of the EI's or:

$$(ea) = \frac{\sum_i^i \overline{EI}_i \bar{a}_i}{\sum_i \overline{EI}_i} \qquad (2.9)$$

where (ea) is the shear center position aft of the leading edge and $\bar{a}_i$ is the position aft of the leading edge of a structural bending element. For the models of this report, the $\overline{EI}$ of the spar is much larger than the $\overline{EI}$ of the balsa covering (the only other structural element of the model), so that effectively the elastic axis lies at the spar position.

With spar position and size known, the mass and center of gravity of the wing section without balancing lead weights can be determined. For the models used in this program two lead weights, generally one fore and one aft of the spar, were used to give the wing section the required total mass properties. Reference 1 gives a good description of the process of design of these lead weights. Trial and error procedure may be necessary for some lead weight designs, but it is straight-forward and can easily be set up in tabular form.

Models with solid aluminum spars, designed in the manner described above, have been quite satisfactory. For the range of torsional frequencies of about 100 cps to 300 cps their static strength has been adequate. No cases of divergence have been encountered. The models are not strong enough to withstand the starting shock associated with the initiation of supersonic flow in the test section. It is therefore essential that the model be injected into the test section after supersonic flow has been established. No major difficulties have occurred during injection. Some buffeting has been encountered on injection, but except for a few models with control surfaces of low natural frequency no damage has occurred on injection of the model.

The models built using the design procedures outlined above are quite light. Relative density, μ, values of from 45-65 have been obtained with relatively

inefficient solid aluminum spars. Using a more efficient spar consisting of a steel or aluminum skin cemented to a pine or balsa core μ values of 20-30 can be obtained in the blow-down tunnel used in this program. Figure 22 shows the range of air density that can be obtained in the tunnel. As can be seen from Fig. 22, the air density depends on stagnation pressure that can be maintained in the settling chamber, the Mach number of the test, and the condition of the air in the pressure reservoir. As can be seen from Fig. 22, sea level density is obtainable in the tunnel only at Mach numbers below 1.5. The limit on air density imposed by the tunnel of course limits the values of relative densities that can be obtained.

Balsa wood, if used as the material for producing the required aerodynamic shape, must be carefully calibrated to determine its density and moduli of elasticity E and G. The structural properties of balsa were found, of course, to vary greatly with grain direction. Each piece of balsa used in the models was carefully calibrated to determine its structural properties. For all the straight and swept wing models built in this program the balsa grain was perpendicular to the elastic axis. For all the delta wing models the grain direction was parallel to the nominal elastic axis. A very satisfactory glue for making balsa-to-metal and metal-to-metal glued joints was the Armstrong A-2 cement. It was also used quite successfully in building spars of metal cemented to wooden cores. Some of these spars experienced violent flutter twice without detectable damage to the bonds. For making wood-to-wood joints, the Borden Company "Elmer's" glue was very satisfactory.

One of the major problems in the construction of the models is their small size. This is particularly troublesome in the construction of control surfaces. The small size is generally dictated by tunnel limitations as discussed in Section 2.4. There is no easy cure for this problem except careful model building.

Models built using the design and construction procedures outlined above have been quite satisfactory for supersonic flutter testing. Their measured properties have agreed quite well with their assumed and designed properties. An improvement which would simplify their construction would be to find a more homogenous and uniform material than balsa wood for the aerodynamic fairing of the models. No experimentation along this line has been carried out on this program, but some foam plastics appear promising. Surface condition might be a problem with foam plastics even more than with balsa, and a smooth covering might have to be used with plastics. The surface condition of the balsa model wings built on this program, even with careful sanding and paintings, are rough enough so that the boundary layer is probably turbulent over the wing. No great

difficulty was experienced in holding the leading edge radius of the balsa wings down to about 0.007 inch. The leading edges are fragile to touch but stand up well in supersonic flow for the short periods involved in flutter testing.

2.2 Static Testing Techniques

This section will cover briefly the various static tests that were made on the models. The static tests are divided into two types. First, those which were made to determine the properties of the model tested considering it to have an elastic axis. These tests involved finding elastic axis position, root bending flexural rigidity EI_o, and root torsional rigidity GJ_o. Second, the determination of a matrix of flexibility influence coefficients for the model tested. The most common instrument for making measurements of static deformations is the dial gage, but the dial gage introduces a spring force on the model (the force necessary to move the gage) which is inconvenient since it makes necessary calibration of the gage itself. Therefore, in the measurement of static deformations on the models of this program no dial gages were used directly on the models. Optical and electromagnetic means of measuring static deformation were used and found to be more satisfactory.

For measuring the properties of the model considering it to have an elastic axis, optical methods were used. Figure 6 is a schematic view of the test arrangement. The wing mounted in a cantilever support is loaded by attaching weights to the loading rig. Figure 6 shows the arrangement for loading the wing in pure torsion. Glass scales are attached to a second rig on the wing, and the movement of the glass scales is observed through a transit. Figure 8 shows the vernier scales that are scribed on the glass scales. Ten parallel vertical lines are scribed on the glass scales. Oblique horizontal lines 0.01 inch apart are scribed as shown in Fig. 8. The intersection of the horizontal transit cross hair with an oblique line and a vertical gives the vernier reading to 0.001 inch. The reading shown in Fig. 8 is 0.572. The glass scales can be used to read deflections to an accuracy of 0.001 inch.

In actually determining the elastic axis position, EI_o, and GJ_o, use is made of the known wing stiffness distributions. For the models built under this program the assumption was made that an elastic axis at constant chord position exists. Measurements were made near the tip station and these were used to find EI_o and GJ_o. Also the position of the elastic axis of the tip station was assumed to be the location of the elastic axis. To find the elastic axis use was made of the definition of elastic axis as the point at which an applied load produces pure bending. The actual process of finding this point involves trial and error, for unless the loading and measuring rigs of Figs. 6 and 7 are perpendicular to the elastic axis, twist

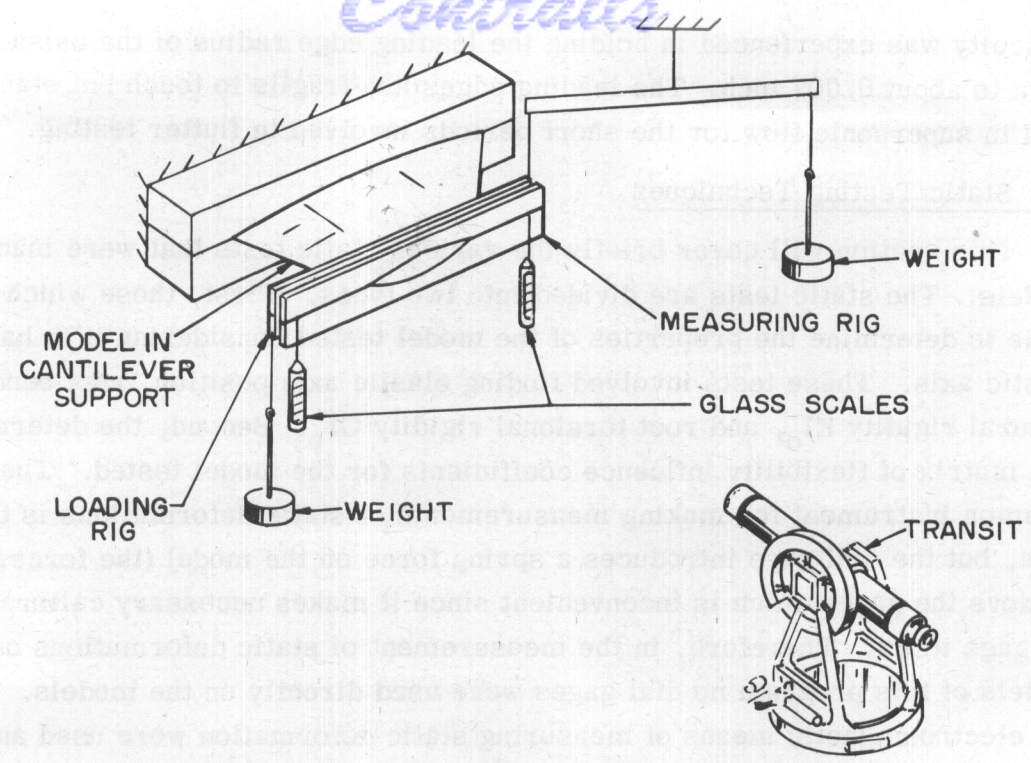

Fig. 6. Schematic diagram of optical system for EI, GJ and elastic axis position measurement.

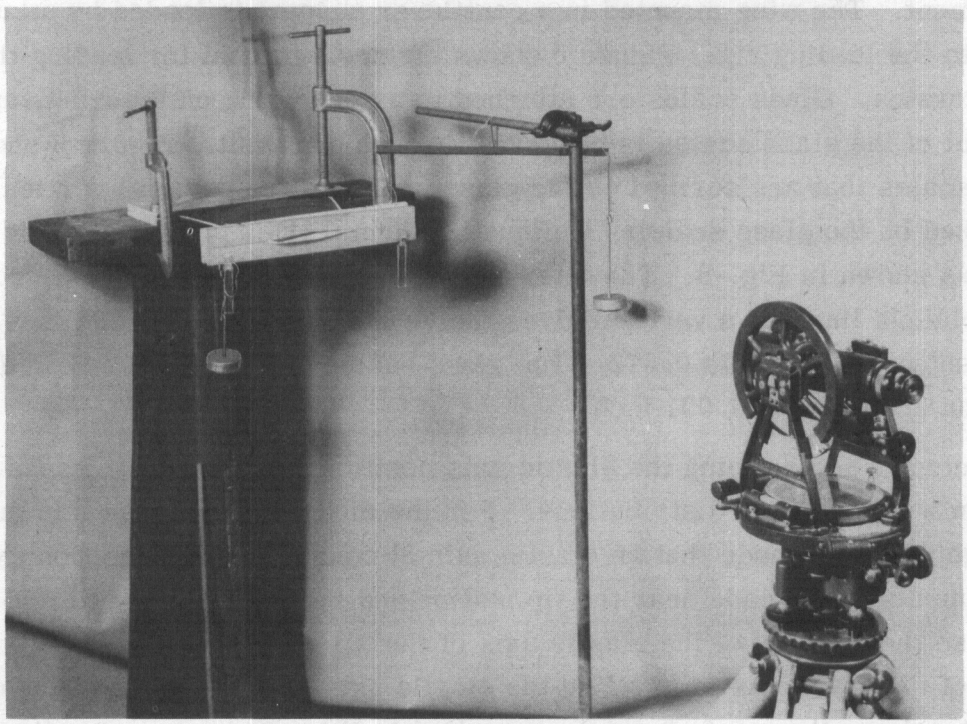

Fig. 7. Glass scale and transit measurement rig.

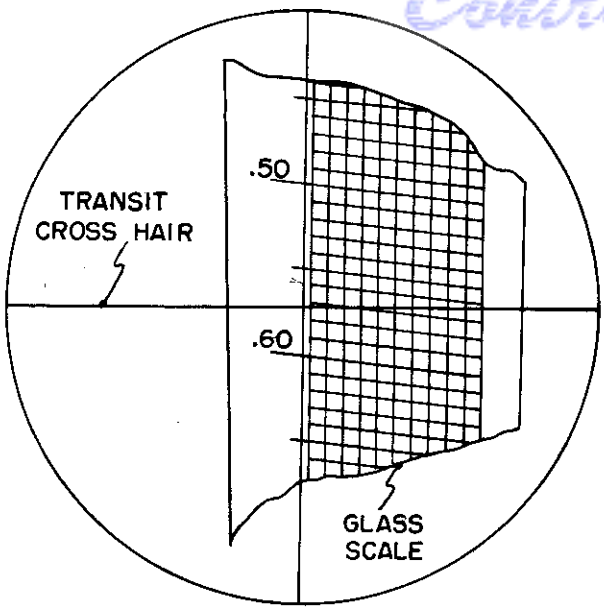

Fig. 8. Glass scale vernier.

will be measured when a load is applied. Fortunately, the process of picking an elastic axis, loading the wing, and finding out whether the assumed elastic axis agrees with the measured one converges rapidly, and in general only a few trials are necessary to find the apparent elastic axis. Once the elastic axis has been found, torsion and shear loads are applied to the tip and the tip deflections are measured. Since the spanwise distributions of EI and GJ are known for the models tested under the present program, their root values may be obtained from formulas of the type:

$$\left|Z_{tip}\right| = \left| \frac{P_{tip}}{\overline{EI}_o} \int_0^{\bar{L}} \int_0^{\bar{L}} \frac{P(\bar{L} - \bar{y})\, d\bar{y}\, d\bar{y}}{[1 - (1 - \lambda)\bar{y}/\bar{L}]^4} \right| \qquad (2.10)$$

and

$$\left|\theta_{tip}\right| = \left| \frac{T_{tip}}{\overline{GJ}_o} \int_0^{\bar{L}} \frac{d\bar{y}}{[1 - (1 - \lambda)\bar{y}/\bar{L}]^4} \right| \qquad (2.11)$$

where $\left|Z_{tip}\right|$ is the absolute magnitude of the tip deflection, under tip load P_{tip} and $\left|\theta_{tip}\right|$ is the absolute magnitude of the tip twist under tip torque T_{tip}. The integrals of Eqs. (2.10) and (2.11) must be adjusted for the fact that neither the actual deflection measurements nor the loading are exactly at the tip of the model because the loading and measuring rigs have finite thicknesses. The integrals of Eqs. (2.10) and (2.11) must also account for these facts.

The method described for finding the static parameters rests on some very broad assumptions, in particular the assumption that the elastic axis exists and has a constant percentage chordwise position along the span. Several models were checked by finding the shear center at various points along the span by the methods described above. The results showed that for the outboard stations the shear center remains at a constant chordwise position to within ± 5% of the chord. The other major assumption that the torsional and bending flexural rigidities vary spanwise as the fourth power of the wing chord was not checked, but the spars, which contribute the major portion of the stiffness, were kept to tolerances of ±0.0005 inch in sectional dimensions. Therefore, it was felt that the actual

variation of EI and GJ was very close to the assumed variation. The actual measured variation in values of elastic axis position, EI_o, and GJ_o for wings that were presumably identical was of the order of ±5% of the chord for the elastic axis position and ±10% of the total value for EI_o and GJ_o.

As noted in Reference 2 the position of elastic axis as determined from the procedure described above may not be too significant since root and chordwise deformations, in swept and delta wings particularly, tend to make the basic assumption of a straight elastic axis invalid. Perhaps a better method of defining the structural characteristics of the models is their calculated shear centers. The shear center could be quite carefully controlled in the design stage as noted in Section 2.1, and for all the models designed for this program the shear center was located at a constant chordwise position along the span. Both calculated shear center and measured elastic axis position are given in the data of Reference 2.

The measurement of flexibility influence coefficients was made using a linear variable differential transformer or Schaevitz coil. (See References 5 and 6.) This device, as its name suggests, is a transformer with a movable steel core. As the core is moved, the output voltage of the secondary coil of the transformer is a linear function of the motion of the core. The Schaevitz coils used in this program had sensitivities of about 0.8 volt per inch per volt primary input at 60 cycles per sec. Two sizes of Schaevitz coil were used, one with a usable linear range of about 0.250 inch and one with a usable linear range of about 0.050 inch. The smaller coils, because of their ease of adjustment, have been most satisfactory for the purposes of this program.

The output of the Schaevitz coils has not been used directly to measure deflections. A null balance system, described in Reference 6 and shown in Fig. 10, was used in order to eliminate the effects of primary voltage change. Figure 9 shows the method of attaching the Schaevitz coil to the model. It also shows the arrangement of the various components of the null balance system. Figure 10 shows the block diagram of the Schaevitz coil null balance system and a simplified wiring diagram for the Schaevitz coils of the null balance system. The measuring coil is attached to the model. When the model is given a deflection δ_{WI}, a voltage V_M is produced which is proportional to the deflection. This voltage is compared with the voltage V_I from the master or indicating coil. The difference voltage $V_M - V_I$ is amplified and used to drive a servo motor which is geared to the indicating coil as shown in Fig. 9. The core of the indicating coil is then driven by the servo motor through the gearing to the same position as the core of the measuring coil. At this point V_M is equal to V_I and the motor stops. The

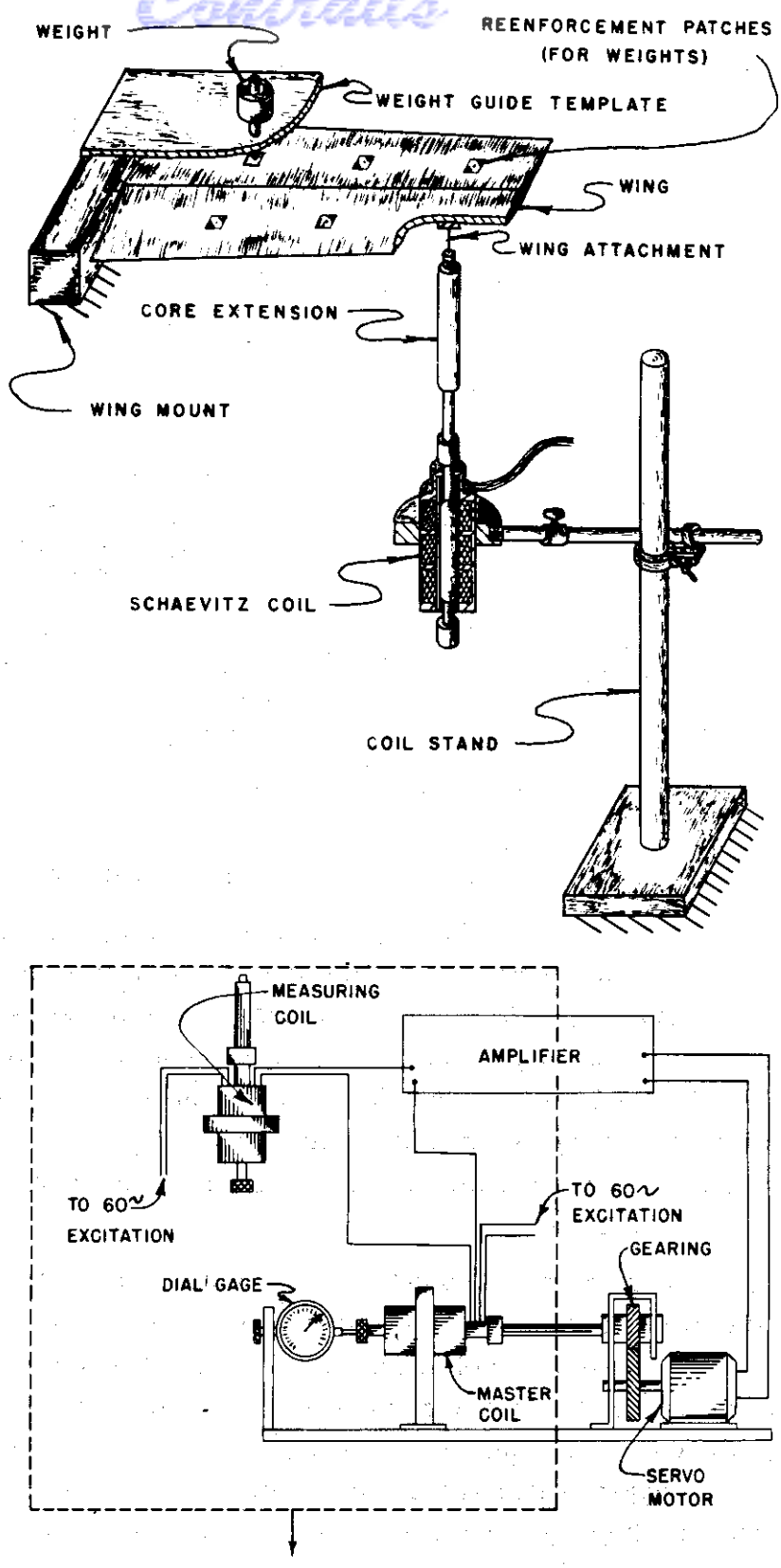

Fig. 9. Setup for static test using Schaevitz coils.

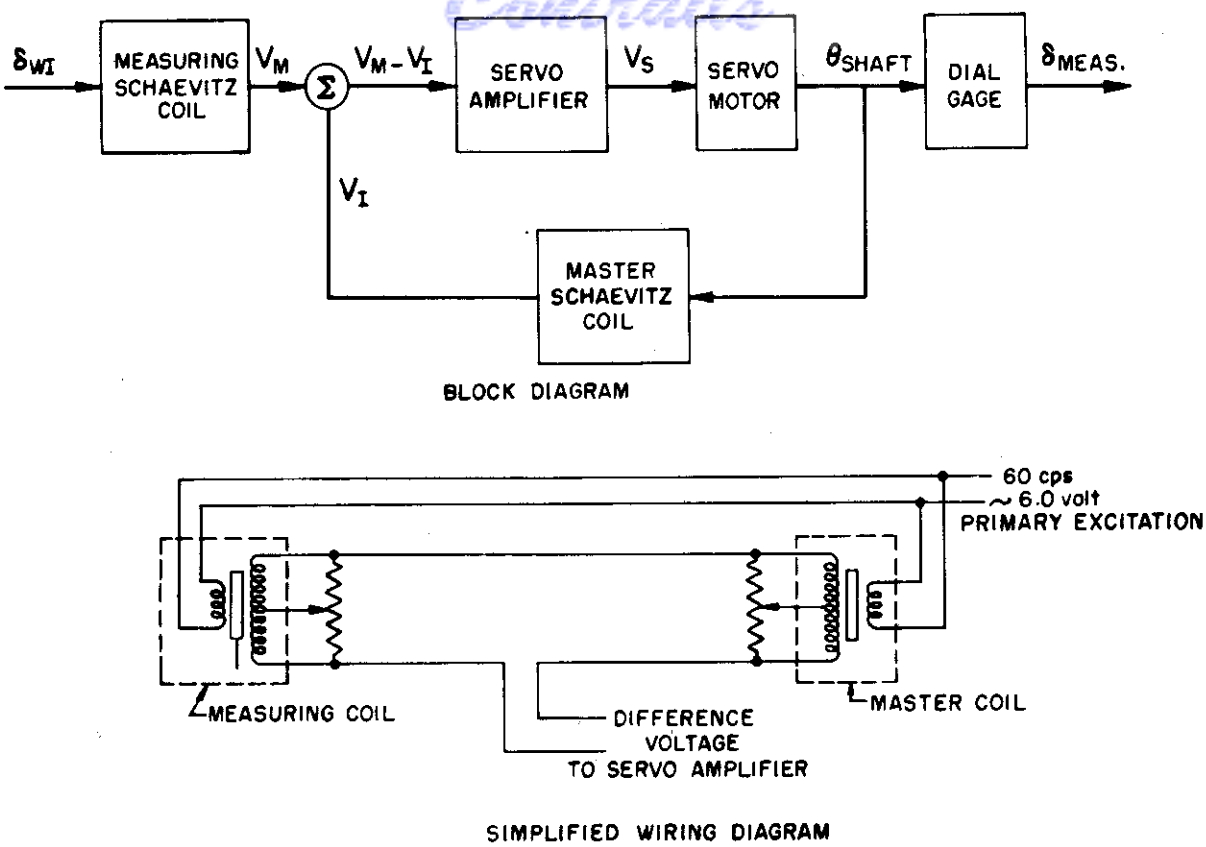

Fig. 10. Block and wiring diagram for null-balance Schaevitz coil system.

position of the core of the indicating coil is recorded by a sensitive dial gage, and so the position of the core of the measuring coil can be recorded remotely by a sensitive dial gage. More than one measuring coil can be attached to the wing at a time, and a simple switching arrangement allows all the measuring coils to be compared one after another with the master coil. A large number of deflections on a wing can then be quickly read. Figure 11 is a photograph of a wing with a number of Schaevitz coils attached for the measurement of flexibility influence coefficients.

The Schaevitz coil can be used where a dial gage cannot directly be used because the force necessary to move the core of a properly adjusted coil is very small, about the order of 0.1 dyne. Care must be taken that the coils are adjusted properly so that the core is centered in the windings. If this is not done properly, the core will drag on the windings, introducing some force on the model. The dragging will introduce considerable hysteresis in the deflection measurements. Improper centering may also change the calibration of the coil and cause inaccurate readings. The problem of core adjustment is one of the most difficult in the use of Schaevitz coils and a steady hand is needed for

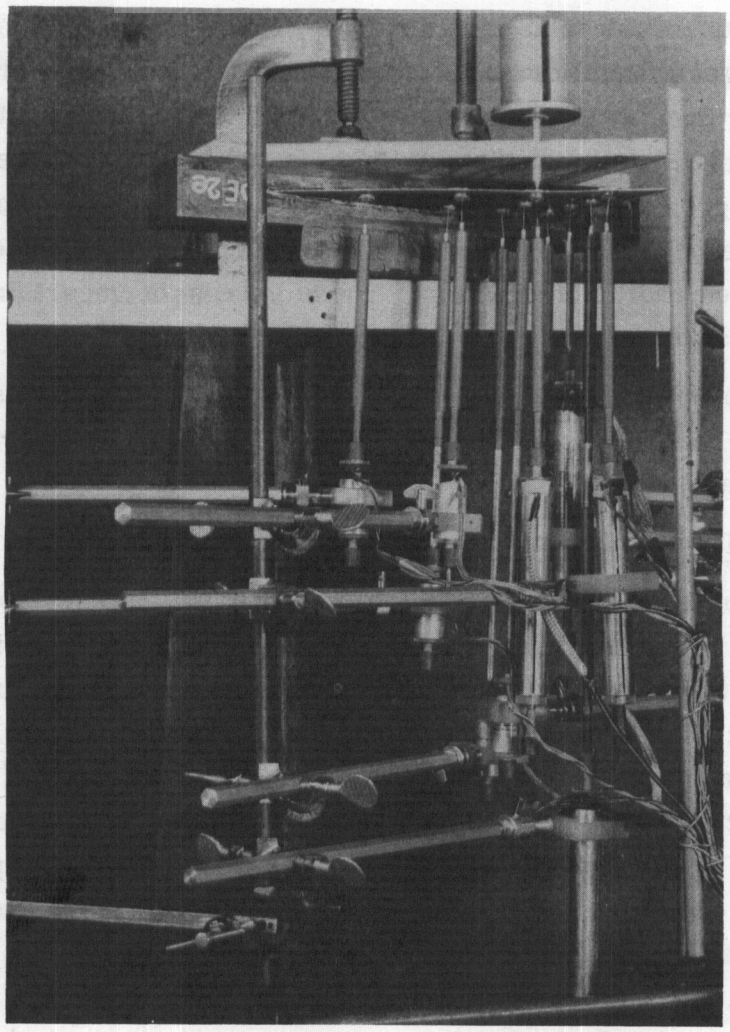

Fig. 11. Delta wing model with Schaevitz coils mounted for flexibility influence coefficient measurement.

adjusting them properly. The presence of ferro-magnetic materials and stray magnetic fields naturally affects the operation of the coils adversely and all supports and core extensions should preferably be made of nonmagnetic materials and stray magnetic fields should be avoided. Considerable experience in the operation of the coils in different locations indicates that calibration checks should be run frequently. Under normal operating conditions the Schaevitz coils have an average deviation of about ±0.0004 inch.

No detailed final check was made on the mass properties of the models. Each element of the wing was carefully weighed before it was put in the model.

It was generally found, however, that the total weight of the finished model was between 5 and 10% of the total design weight greater than the design weight. This increase in weight probably represents the weight of glue and paint in the wing. An attempt was made to take account of this increase of weight during the design process. It is estimated that the maximum uncertainty introduced into the sectional mass properties of the wing by the glue and paint is about ±3% of the mass per unit length, ±2.5% of the chord in center gravity position, and about ±5% in the section radius of gyration. These maximum uncertainties occur at the tip stations of the model.

The mass properties of tip tanks were measured. Total mass and center of gravity position were measured directly. Mass moments of inertia were measured with a bifilar pendulum.

2.3 Vibration Testing Techniques

Zero air speed vibration tests were made for all the model wings. Mode shapes obtained were cantilever modes. Two methods of excitation were used to obtain the vibration mode shapes and frequencies; excitation of the wing by an electromagnetic shaker attached to the mounting block which can be seen in Fig. 14, and through the use of pulsing air jets on the wing model itself. The electromagnetic shaker was used for exciting frequencies of about 20 cps and more. The air jet excitation was used at frequencies below 20 cps. Since only the models with tip tanks had frequencies below 20 cps, the majority of vibration tests were made with the electromagnetic shaker.

The theoretical considerations which allow determination of the cantilever modes of the model from the vibration test setup of Figs. 13 and 14 are easiest seen from the simple two-degree-of-freedom system illustrated by Fig. 12.

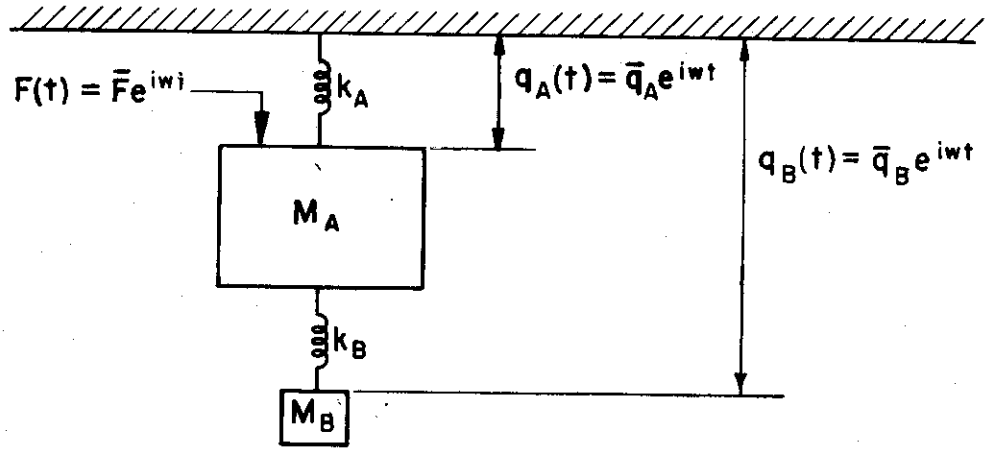

Fig. 12. Two-degree-of-freedom spring-mass system.

Let M_A and M_B be the masses, k_A and k_B the spring constants, $q_A(t)$ and $q_B(t)$ the displacements of the masses, and $F(t)$ a force acting on M_A. The barred quantities are the complex amplitudes. The very simple analysis of this system shows that the two natural frequencies of this system are given by:

$$\omega_{1,2}^2 = \frac{[\omega_A^2 + \omega_B^2 (1 + \frac{M_B}{M_A})] \pm \sqrt{\left[\omega_A^2 + \omega_B^2 \left(1 + \frac{M_B}{M_A}\right)\right]^2 - 4\omega_A^2 \omega_B^2}}{2} \tag{2.12}$$

where

$$\omega_A^2 = \frac{k_A}{M_A} \tag{2.13}$$

and

$$\omega_B^2 = \frac{k_B}{M_B} \tag{2.14}$$

The frequencies ω_A and ω_B are the natural frequencies of each spring-mass system by itself. If $M_B \ll M_A$ then Eq. (2.12) shows that the two natural frequencies, ω_1 and ω_2, of the system of Fig. 12 are ω_A and ω_B. It can also be shown that if the frequency of the exciting force $F(t)$ approaches ω_B, the amplitude of motion $\bar{q}_A$ approaches zero while the amplitude $\bar{q}_B$ remains finite but large. If the frequency of the exciting force approaches ω_A, then both $\bar{q}_A$ and $\bar{q}_B$ are approximately equal and finite provided that $\omega_A \ll \omega_B$.

This simple system just discussed is similar to the vibration test setup shown in Fig. 13. The simple $M_B - k_B$ system of Fig. 12 is replaced by the wing which has a large number of degrees of freedom. All of these wing structural degrees of freedom have much higher frequencies than the frequency of the wing in its support block and vibration rig support plate on its soft springs. This latter system corresponds to the $M_A - k_A$ system of Fig. 12. Furthermore, the mass of the support plate and block is much greater than that of the wing. If a sinusoidal force is applied to the support plate by electromagnetic shakers and the frequency of this applied force varied, then, by analogy with the simple system of Fig. 12, each of the natural cantilever vibration modes of the wing will

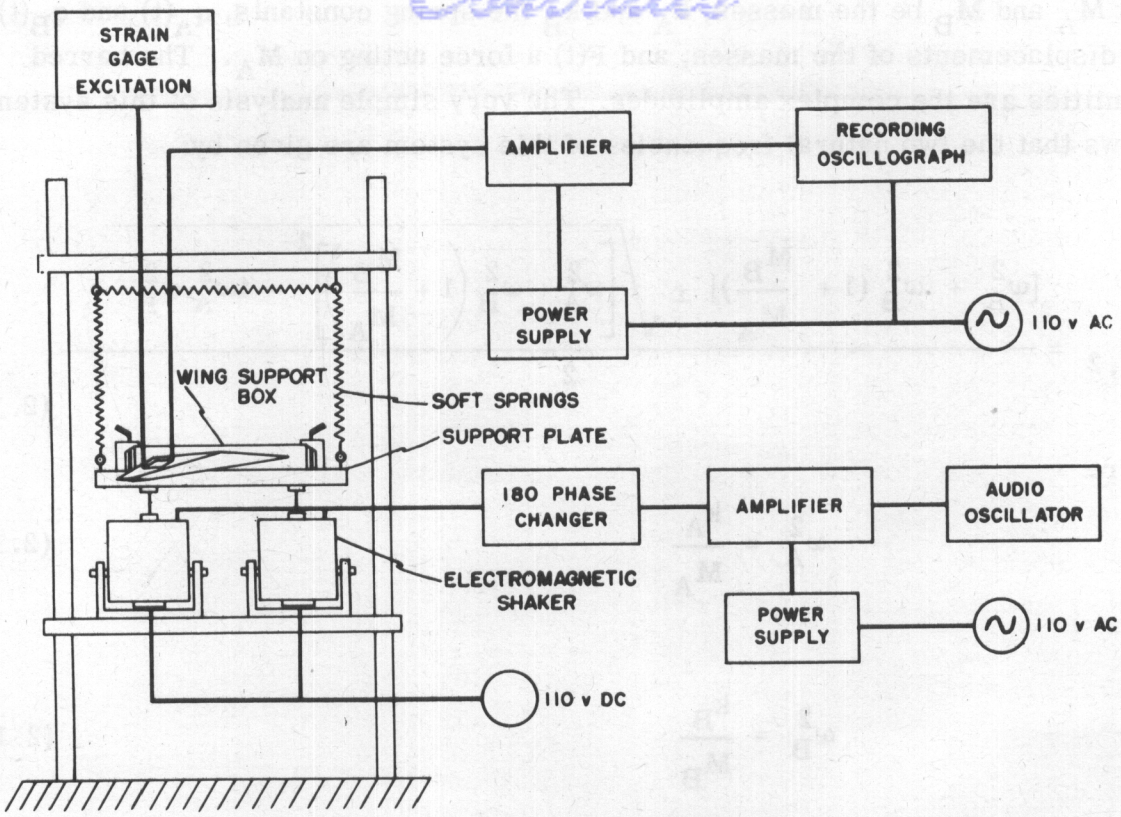

Fig. 13. Setup for vibration test using electromagnetic shaker.

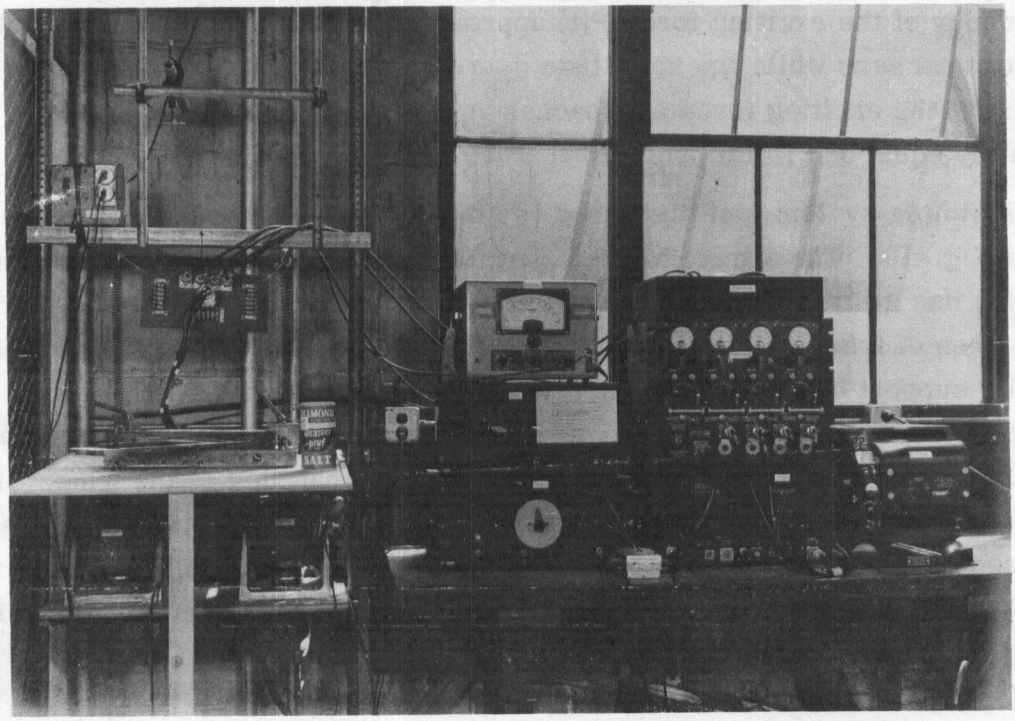

Fig. 14. Vibration test rig and recording equipment.

be excited as the frequency spectrum is traversed. The approach of each mode can be detected by watching the output of strain gage bridges on an oscilloscope. When the frequency of each mode is reached, the amplitude of the strain gage trace will grow rapidly. To excite bending modes a force is applied to the support plate, and the two electromagnetic shakers of Fig. 13 are operated in phase. To excite torsional modes a moment is applied to the support plate, and the shakers are operated 180° out of phase.

Simply exciting the mode by the shakers may not find the correct frequency since the response of the wing and wing-support – plate system will have a frequency equal to the frequency of the exciting force or moment. If, however, the exciting force is abruptly cut off, the model motion will decay at a frequency very close to the natural frequency of the model. The difference between the natural frequency and the decay frequency is caused by the structural damping g as noted in Reference 7. However, for values of g less than 0.03 the change is less than the experimental uncertainty. If the decay is recorded the damping coefficient g can be found from the record of the decay. Reference 7 gives g as:

$$g = \frac{0.22}{N} \tag{2.15}$$

where N is the number of cycles required for the record to decay to one half amplitude. Figure 15 shows a vibration record from the oscillograph. Two strain gage bridges were used on this model. One bridge recorded bending strain at the root of the spar, the other torsional strain at the root of the spar. The record of Fig. 15 shows that the mode excited was primarily torsion. The decay on this record is very good and frequency and g can easily be found from the record. The frequency can generally be obtained to ±0.5 cps and the g's to within ±.005. These uncertainties vary with the quality of the record and the number of cycles that can be counted to determine both frequency and g.

The position of the nodal lines for each vibration mode was determined along with the frequency and damping g. The nodal lines were determined by sprinkling ordinary table salt on the wing. When a vibration mode is excited the salt is shaken off those portions of the wing where the acceleration is greater than the acceleration of gravity. With reasonable amounts of amplitude in the mode, the salt then remains only at the nodal lines of the vibration mode. Pictures of the nodal lines for the first four modes of a swept wing model are shown in Fig. 16. After the nodal lines have been found from the salt they can either be photographed, carefully sketched, or traced on vellum for a permanent record. No attempt was made to define the natural mode shapes beyond recording the node lines.

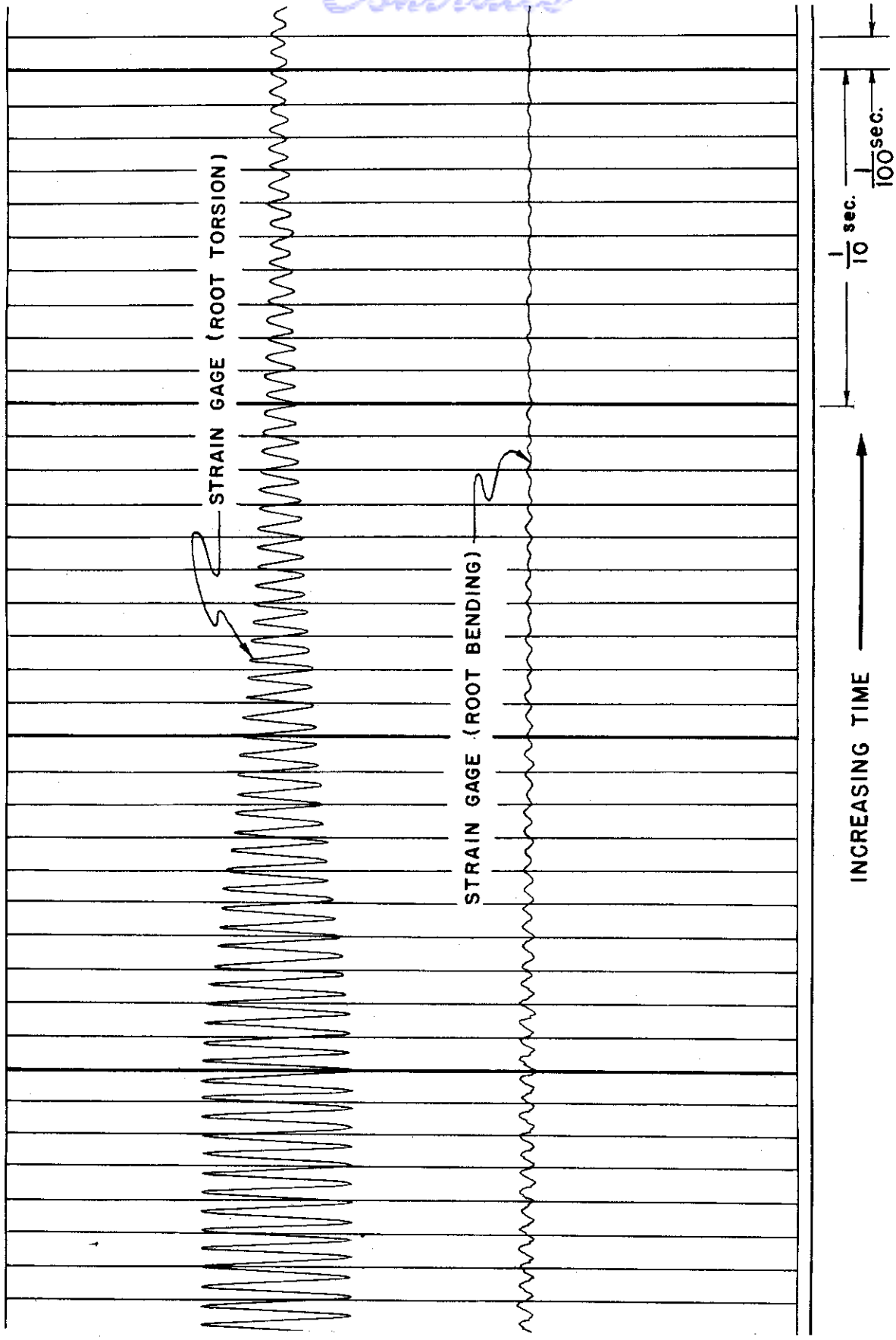

Fig. 15. Sample vibration record.

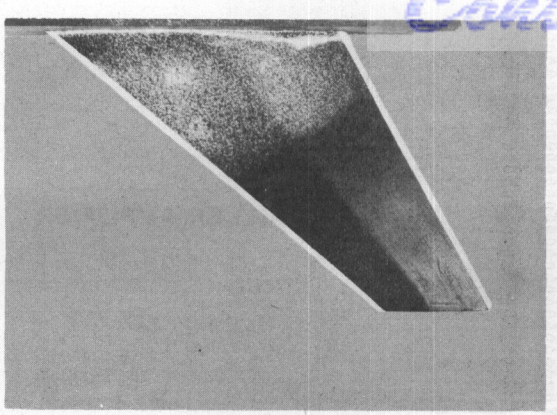

First Bending

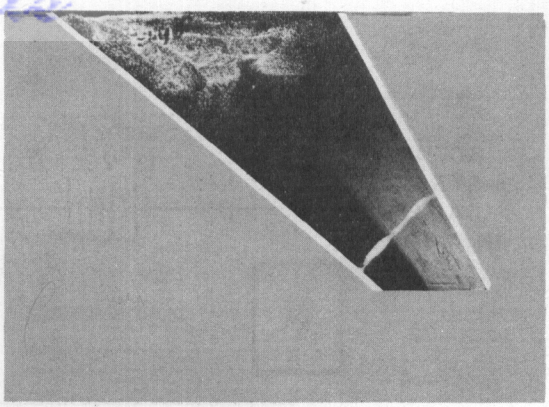

Second Bending

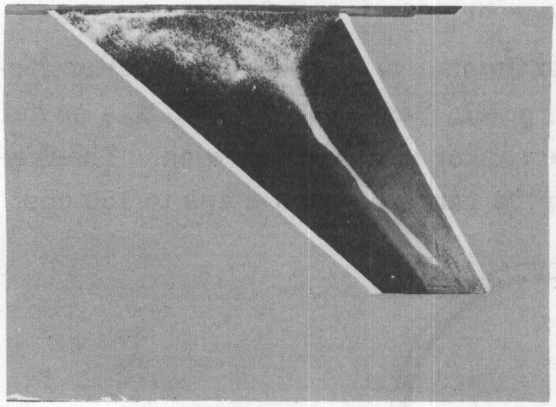

First Torsion

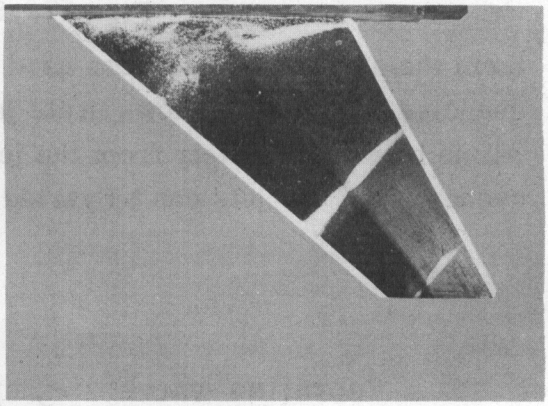

Third Bending

Fig. 16. Nodal lines for swept wing.

The strain gage bridge excitation of Fig. 13 is a 12 volt battery. The wiring diagram for the strain gage bridge is shown in Fig. 17. This DC-excited two-arm bridge has a number of advantages for practical flutter testing where only frequency and damping are desired from the strain gage records. Steady strains are not recorded which is an advantage since static airload deformations are eliminated from the flutter records. Because steady signals are not transmitted through the transformer, the bridge need not be balanced too carefully. If a gage in the model becomes inactive, it can quickly be replaced by a dummy resistor without careful balancing of the bridge. This is a great advantage in flutter testing where gages may be easily over-strained and broken.

For models with vibration frequencies below about 20 cps, the electro-magnetic shaker rig cannot be used since the frequency of the natural modes becomes too close to the frequency of the model support box and support plate on the soft springs. These models were those having tip tanks and weights. For

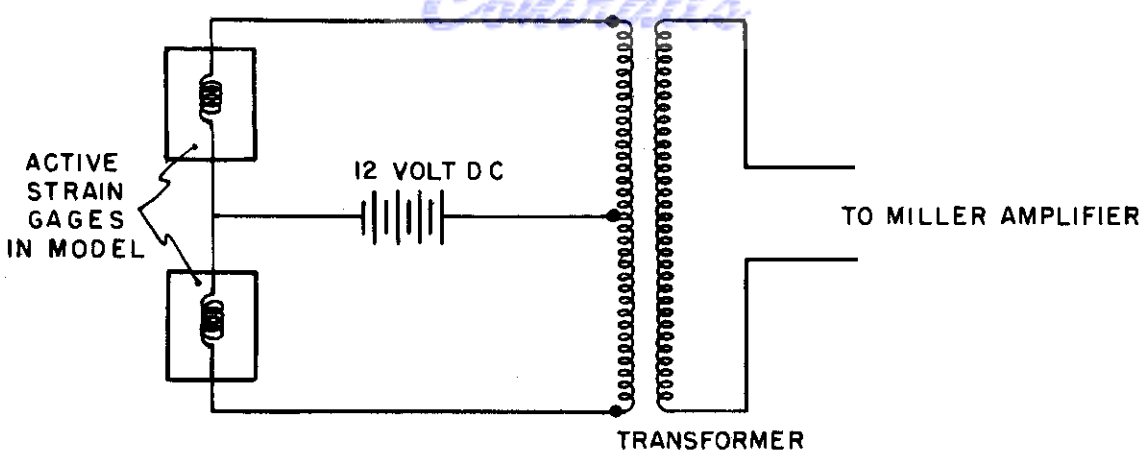

Fig. 17. Strain gage bridge.

them the air jet shakers were used to excite the natural cantilever vibration frequencies. Figure 18 shows an air jet shaker unit in position on the tip of a model. Air is blown alternately from the jets of the shaker unit onto the wing. The frequency of the air jets can be varied through the range of about 2 cps to 150 cps,

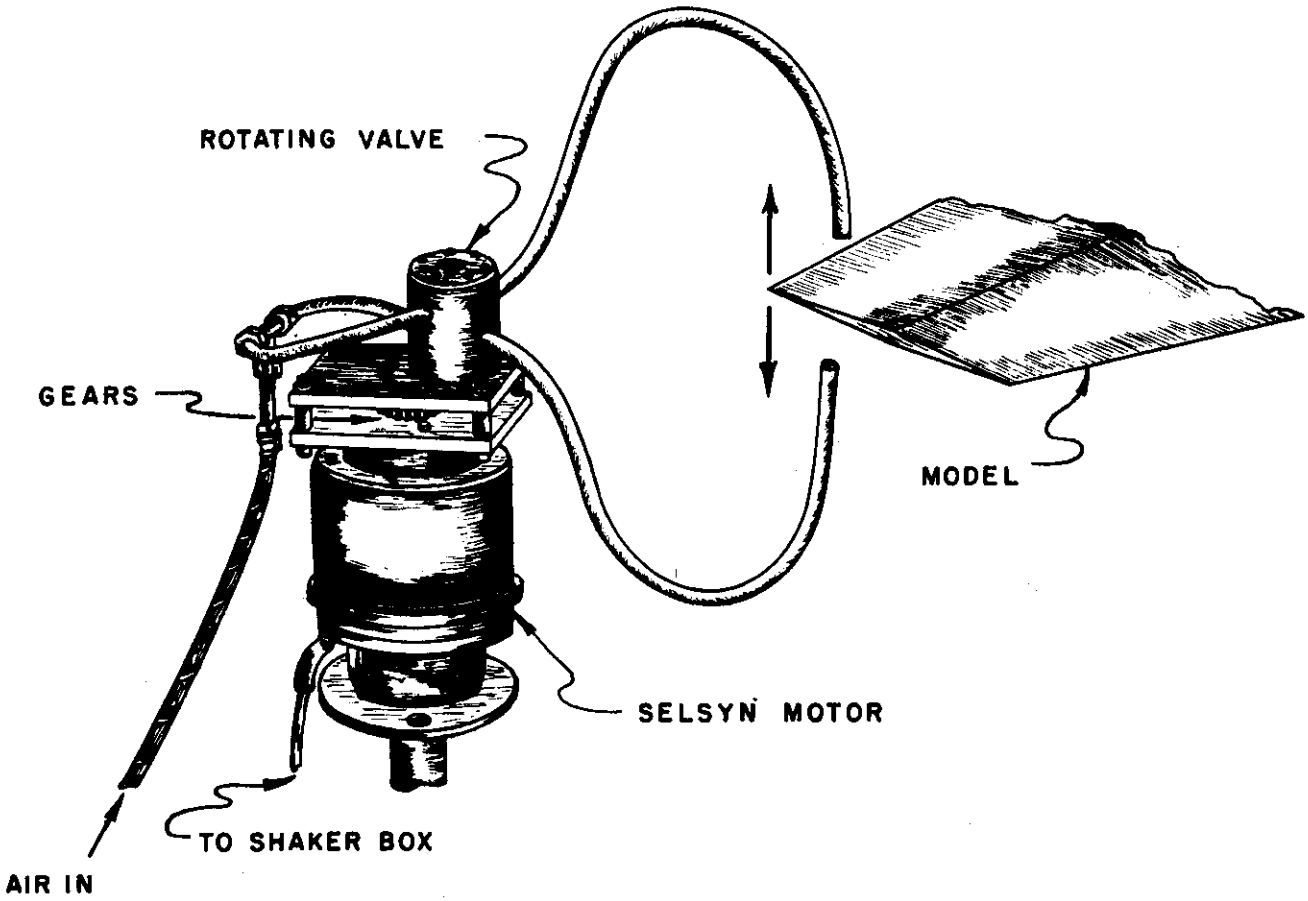

Fig. 18. Air jet shaker unit.

though the air jet shakers were not used for frequencies much above 75 cps. The model is clamped in a cantilever support, and the cantilever frequencies, dampings, and nodal line positions can be recorded by strain gages in the same manner as with the electromagnetic shaker rig of Fig. 14. The air jet shaker has the great advantage of exciting the wing from an outboard location without introducing appreciable mass which will disturb the mass distribution of the wing. Simply connecting an electromagnetic speaker core at the outboard portion of the wing, for example, makes the voice coil and its mass a part of the wing mass system. This added mass will, of course, disturb the wing vibration modes.

References 10 and 11 give a description of the air jet shaker equipment. Figure 19 shows a simplified block diagram of the equipment taken from Reference 11. The heart of the system is the interrupter valve which directs sinusoidally pulsating air jets onto the model. The valve is driven, through gearing, by a selsyn motor which follows a second selsyn mounted in the control unit. The speed of this second selsyn, the selsyn driver of Fig. 19, can be varied thus varying the speed of the interrupter valve and hence the frequency of the pulsating jets on the model. Air is supplied to the interrupter valve through a reduction valve mounted in the control unit.

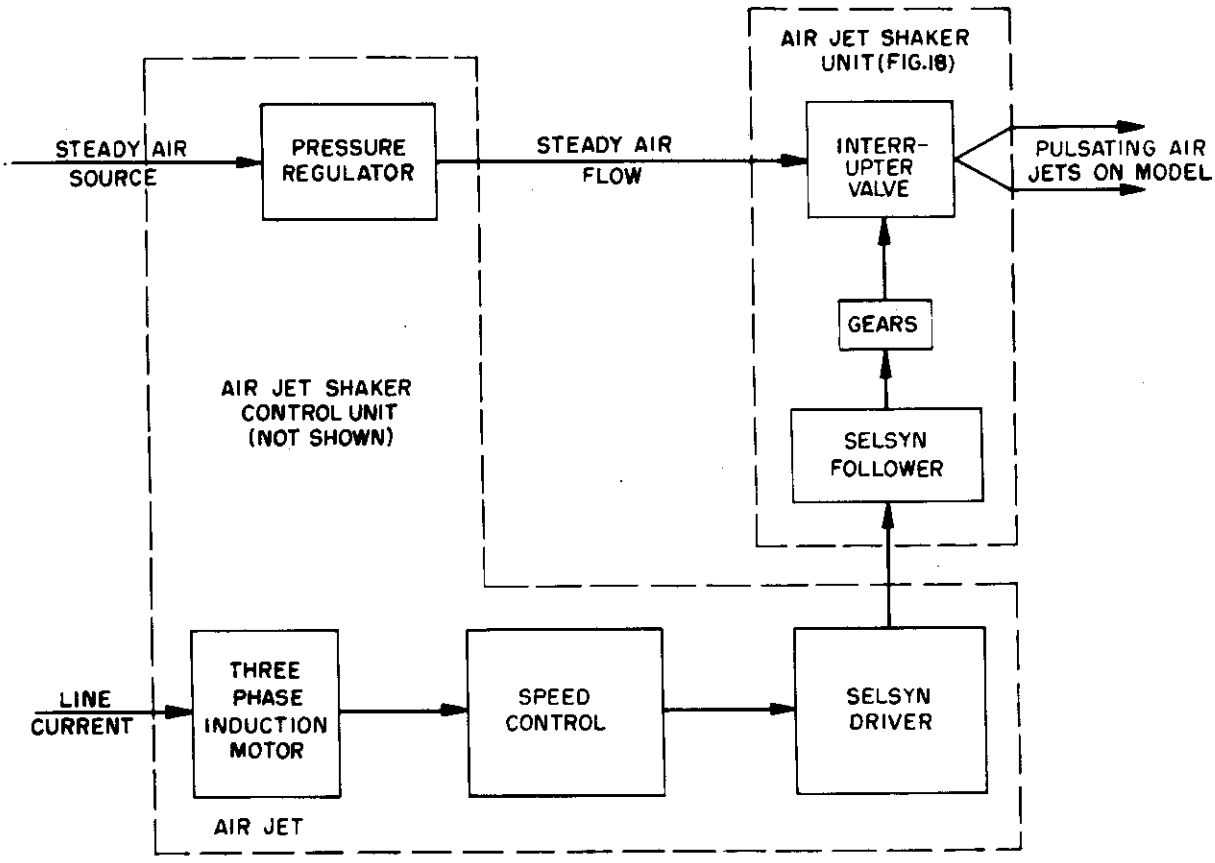

Fig. 19. Block diagram for air jet shakers.

The methods described for vibration testing of the models of this report have been quite satisfactory. The methods cover a spectrum of vibration frequencies from about 2 cps to 1000 cps. At the high frequency end of the spectrum the electromagnetic shaker system as shown in Fig. 13 may have some difficulties because there may be secondary frequencies in the vibration support rig in this range. If these exist, as can be seen by the analogy of Fig. 12, they may disturb the shape of the wing cantilever node lines, and change the frequency of the wing modes.

For the vibration data, several attempts were made to measure the complete mode shapes of the wings. Optical methods using a stroboscopic light were not too successful. An attempt to produce an accelerometer having a weight of 0.20 gram or less using piezoelectric sensitive elements were not successful. The weight of the accelerometer finally built was too great to be attached to the wing without disturbing the mass distribution. It is suggested that such accelerometers might be built into the model and their weight accounted for in the design process. This would, however, limit the measurement of mode shape to a few positions on the model. The quantitative measurement of mode shapes, particularly for the delta wings where the interaction of second bending and torsional modes seems very important, would be a great advantage.

2.4 Flutter Testing Techniques

When the program of supersonic flutter testing reported on in this series of reports was initiated, not too much was known about flutter testing in the supersonic range. It was early realized that the light weight models of this program would have to be injected in the supersonic airstream because the starting shock associated with the tunnel would destroy the models before supersonic flow was established in the test section. This need was made very clear during the test program, when some models, of all planforms, were injected in advertently into the tunnel before the starting shock had passed downstream of the test section. Except at very low Mach numbers, the starting shock destroyed the model. The fact that models must be injected quickly into the supersonic flow does not lead, however, to any special requirements on the model except when control surfaces or tip weights are attached to the model. In such cases buffeting on injection causes some problems of keeping the control surfaces and tip tanks attached to the wings.

Model size requirements are limited by the reflected shock pattern in the test section. It is desirable to keep the model inside the shock and Mach wave pattern formed by the model and the reflected waves from the tunnel walls. If this is done for supersonic flow, there is no tunnel wall interference. Also a

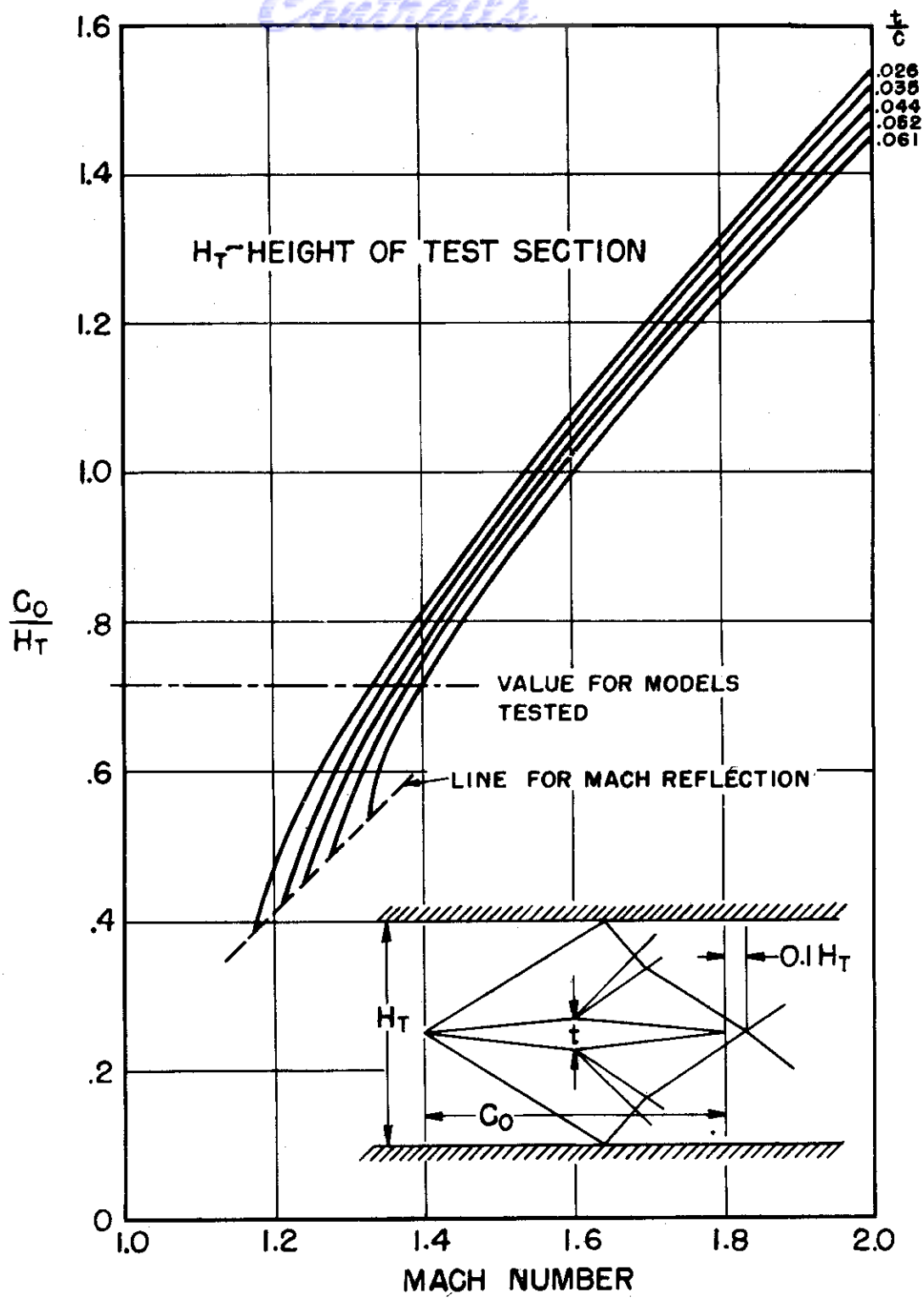

Fig. 20. Allowable root chord as determined by the two-dimensional shock wave pattern.

reflected shock impinging on the model would cause undesirable vibrations and if the shock were strong enough even damage the model. For the half-span models of this program the most critical shock reflection seems to be the reflection of the two dimensional shock at the root of the wing. Figure 20, taken from Reference 8, shows the allowable root chord for the double wedge airfoil models of the present program for a number of thickness ratios. Plotted is the root chord to test section height ratio which allows the reflected shock to intersect the model chord extension 0.10 of the test section height aft of the trailing edge. This represents a margin of safety for shock reflection hitting the trailing edge of the model. Figure 20 shows that the 10 inch root chord 6% thick models of this program, with a ratio of root chord to test section height of 0.714, will be in danger of encountering reflected shock waves on the trailing edge at the root at a Mach number of about 1.4. This value of Mach number for shock interference is probably conservative, and experience has shown that no serious shock wave or Mach reflections occur at Mach numbers down to about 1.3, which is effectively the lower limit of the tunnel operation. (See Reference 9.)

All the flutter testing done on the present program was done in the supersonic blow-down tunnel described in Reference 9. This particular tunnel is ideally suited for flutter testing since the Mach number is continuously variable during a test over a range of Mach numbers from about 2.10 to about 1.30. A flutter point may then be found by varying the flow parameters rather than the model parameters. Figure 21 shows a hypothetical flutter boundary for the whole range of Mach numbers. Figure 21 also shows a tunnel operating curve, which is the curve a model of a given size and ω_α would follow in the tunnel. It can be seen from Fig. 21 that a model in supersonic flow, moving along a tunnel operating curve, approaches the flutter boundary from high Mach number if it is to go from a stable to an unstable region. So all models in the present program were

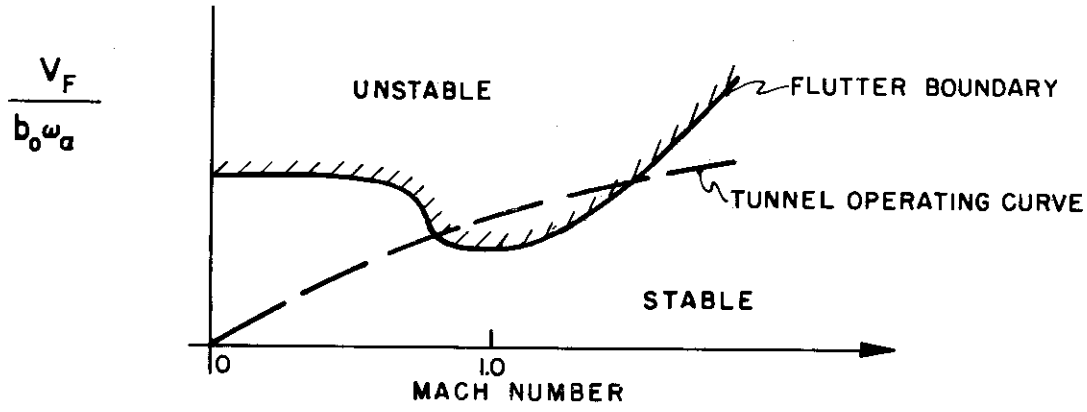

Fig. 21. Hypothetical flutter boundary.

injected into the tunnel at high Mach number and the Mach number decreased until flutter was reached. The method was successful as the results of Reference 2 indicate.

In flutter testing a very important parameter is the relative density, μ, defined for the purposes of this report as $m/\pi\rho\ b^2$ where ρ is the air density, and b is semichord of the wing. Since air density enters the expression for μ, air density is important. Figure 22 shows the range of air densities that can be obtained in the blow-down tunnel of Reference 9. The tunnel can be operated only at constant stagnation pressure, p_o. Therefore, for a given run the density increases as the Mach number is decreased. Stagnation temperature is held roughly constant during a flutter test. The increase in density means that μ is decreasing during a flutter run, and none of the flutter tests were made at constant values of μ. The variation in μ can be decreased by decreasing the Mach number range of a given test. In some tests of the program this was done, and each model was flown through two overlapping Mach number ranges. The variation of μ with Mach number during a run does not affect the validity of the flutter results obtained, but it explains the variation in μ at flutter encountered in some of the data of Reference 2. With the range of densities available in the tunnel, it appears feasible to build models of the type discussed in this report with μ ratios as low as 20 for the low Mach number ranges.

In an actual flutter test the tunnel variables that are recorded are stagnation pressure and temperature, sliding block position, and static pressure from a static pressure cone located just aft of the test section (see Reference 9). From stagnation pressure and temperature, stagnation density can be calculated. From the record of block position, Mach number in the test section can be found. Isentropic channel flow relations can then be used to calculate density, velocity, static pressure, and temperature in the test section. The static cone pressure measured by the static cone just aft of the test section is not used in the reduction of the flutter data, but it serves to tell when the starting shock has passed downstream of the test section, since there is a marked drop in static pressure once the starting shock has passed and supersonic flow has been established in the test section. As noted earlier it is very important to know when supersonic flow has been established since premature injection of the model will result in its loss due to the starting shock. A continuous record is made of the tunnel variables on a recording oscillograph.

The signals from two strain gage bridges mounted on the model spar are recorded along with the tunnel variables. In general, two strain gage bridges were used; one recording root bending strains; the other recording root torsion

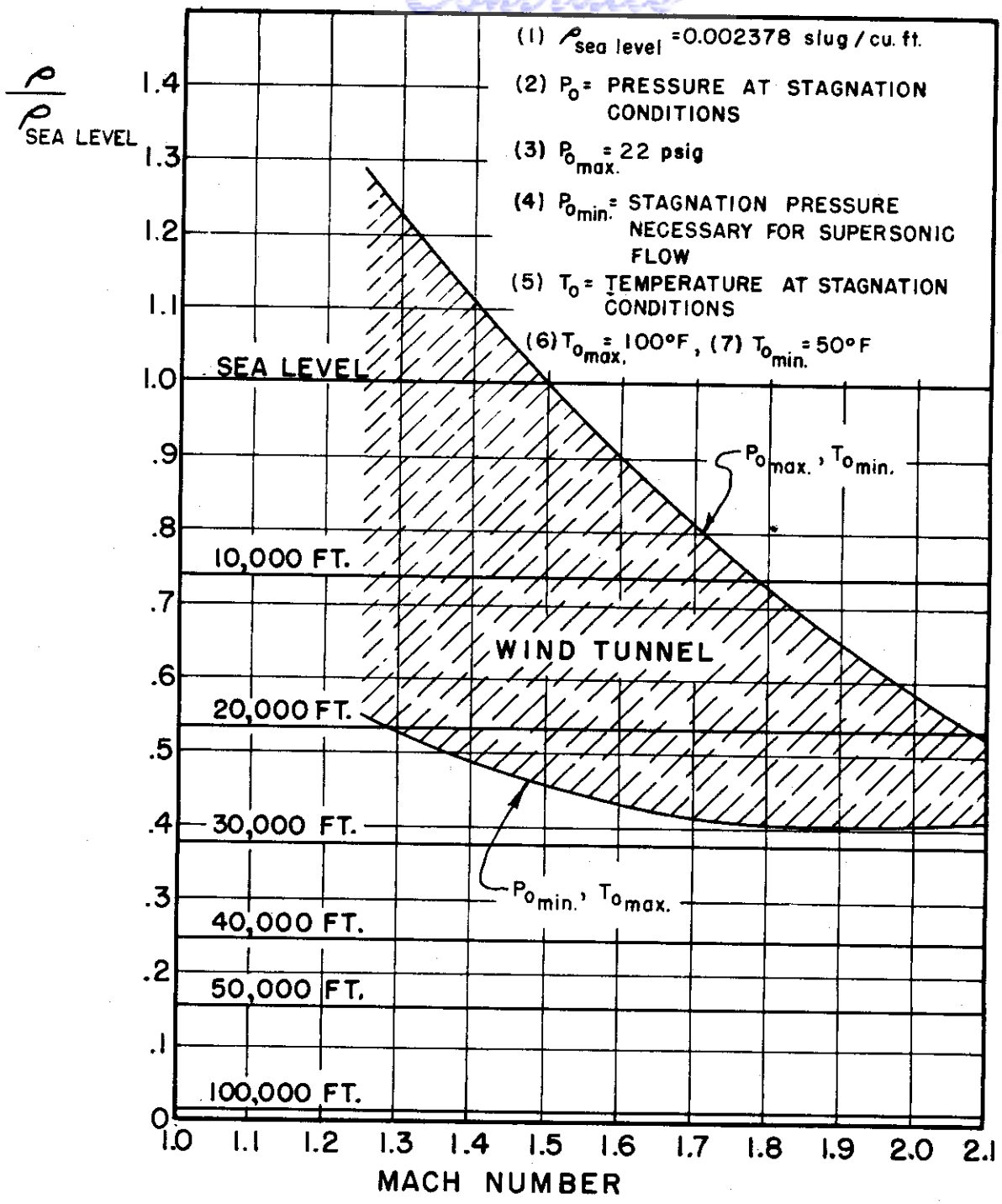

Fig. 22. Density versus Mach number for extreme ranges of atmospheric and wind tunnel conditions.

strains. For models with control surfaces or tip tanks or for models that were free-to-roll added strain gages were used. For control surfaces, a strain gage bridge recording the relative motion of the wing and the control surface was used. For the tip tank models, strain gage bridges recording the strains at the tip of the spar were used. For the free-to-roll models a strain gage bridge measuring roll angle was used. Free-to-roll models were prevented from diverging in roll by canting the hinge as noted in Reference 2. A section of a typical oscillograph record just before and during flutter is shown in Fig. 23. The rapid growth of the strain gage traces is shown. No attempt has been made to correlate the amplitude of the strain gage traces to the amplitude of motion. Only frequency of flutter was obtained from the record. The rapid divergence of the strain gage traces of Fig. 23 is typical of supersonic flutter. The model is generally destroyed in less than 0.1 of a second. There is consequently little chance of saving the model except by developing a very fast flutter brake. No attempt was made to develop such a brake on the present program. The smooth variation in the tunnel parameters is shown in Fig. 23. Notice that the block position and hence all the other tunnel parameters are continuously varying through the flutter. This means that, if the strict view is kept, only the very onset of the flutter represents the actual boundary. However, in 0.10 second the Mach number has only changed by 0.01 which is within the limits of the experimental accuracy. It should also be noted that about 100 chord lengths of air pass the wing for each 0.01 change in Mach number, so that as far as Mach number changes are concerned the flow is steady state.

The measurements of Mach number have an average deviation of about ±.006. Measurements of velocity have an average deviation of about ±5 ft/sec. Measurements of density have an average deviation of about ±0.00001 slug/ft^3. Flutter frequencies are accurate to about 1 cycle per second, but their accuracy depends to a large extent on the quality and duration of the oscillograph record of flutter.

The mode shape of flutter and the amplitude of flutter were recorded by making high speed motion pictures of the models. A Wollensack Fastax camera was used. High speed movies were taken at the rate of about 3000 pictures per second. With a 200 foot roll of film the camera is on for about 7 seconds. This is just about the time necessary to complete a flutter test. Careful synchronization between the time of model injection and the time of starting the camera is necessary otherwise portions of the flutter run are not recorded by the camera. The photographs were taken through the side window of the tunnel as shown in Fig. 24. A periscopic arrangement of mirrors allows a Mach number scale on the sliding block of the tunnel to be seen in the high speed movie. High intensity lights are mounted above the test section and project light down on the top surface

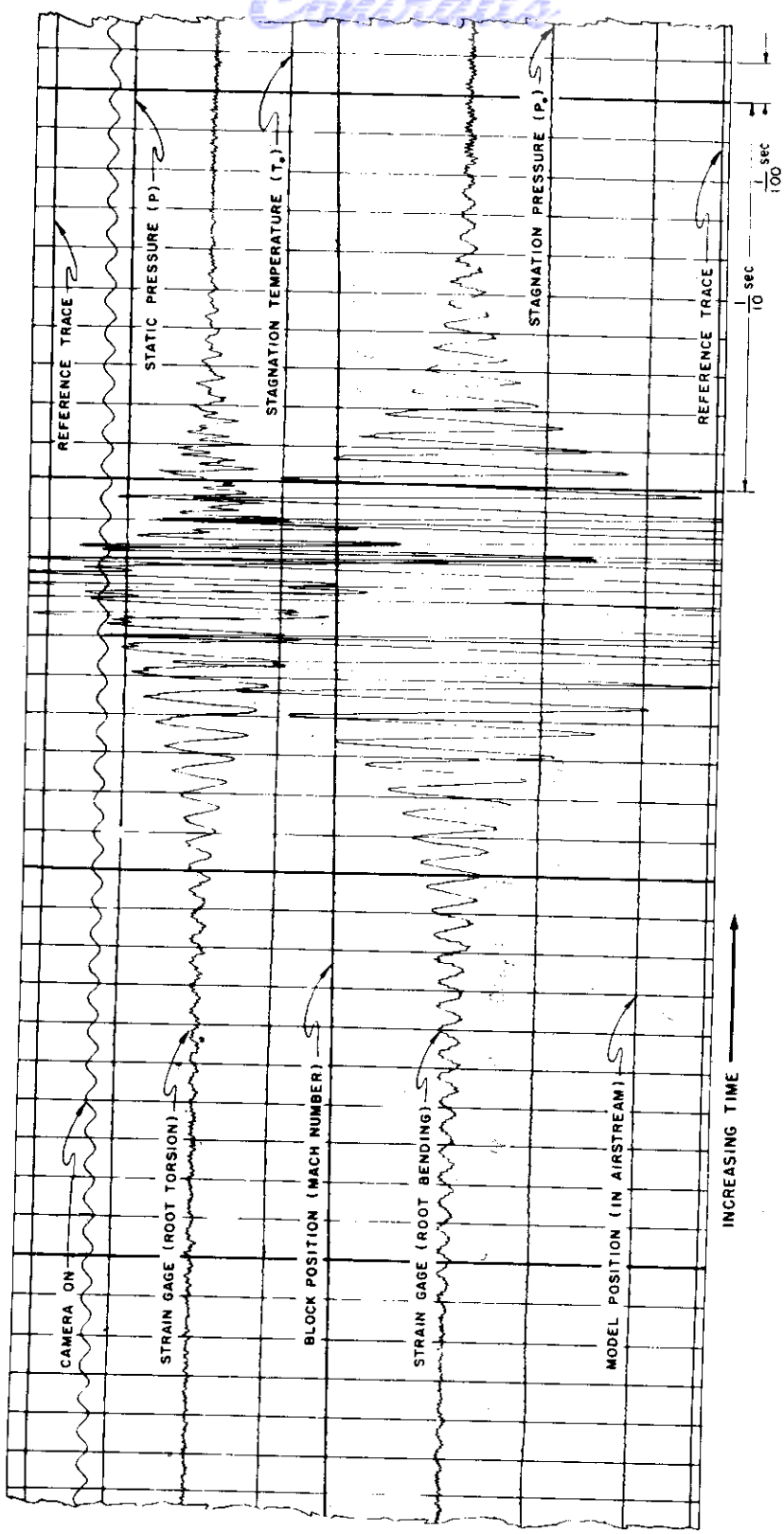

Fig. 23. Typical flutter record.

of the model. The intensity of the incident light on the model must be of the order of 40,000 candlepower to obtain good high speed pictures. An alternate arrangement of the high intensity lights is to direct them through the side window, but objectionable reflections are sometimes obtained with this arrangement. Surprisingly enough, the deep shadow under the wing with the top lighting arrangement shown in Fig. 24 is not objectionable since the wing tip is adequately

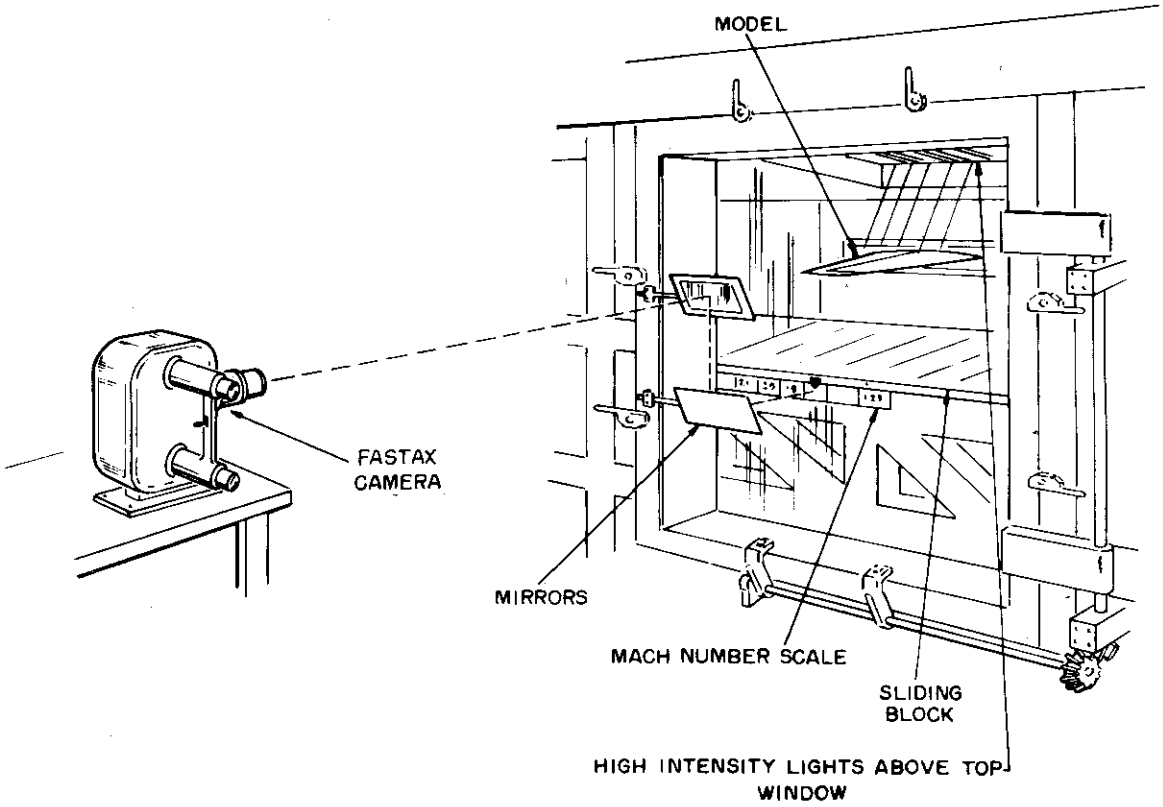

Fig. 24. Arrangement of camera for high speed photography.

lighted and the shadow gives a good contrast to the top and bottom surface of the wing during flutter. Analysis of the high speed photographs to determine amplitude and character of motion during flutter has been made, but, in general, only the tip motion can be measured. Deformation of points on the wing other than the tip are difficult to measure from the high speed motion pictures, and so it does not seem feasible to find the complete flutter mode shape from them. Some of the high speed motion picture analyses are presented in Reference 2. Control surfaces do not show up too clearly on the high speed movies because of the "graininess" of the Tri X film used. A close-up lens, not available for the present program, would help in taking high speed movies of the flutter of control surfaces.

SECTION III

CONCLUSIONS AND RECOMMENDATIONS

As noted in Section 2.1 the model design and construction techniques were satisfactory. Models could be constructed easily and inexpensively. Chordwise deformations were small, but some of the flutter data of Reference 2 indicates that even these small deformations may be important. It may therefore be desirable to stiffen the models in a chordwise direction. For the models of this program chordwise stiffening was necessary on some aileron models at the hinge attachment points. One method of chordwise stiffening is to cement chordwise metal strips to the outside of the balsa fairing. Another method might be to put metal ribs in the balsa. If properly designed, chordwise stiffeners will not change the spanwise wing properties excessively.

The most satisfactory method of making accurate static deflection measurements without disturbing the model used the Schaevitz coils. A satisfactory null balance system was not developed until late in the test program, and so the fullest use of the coils was not made. The standard deviation of these measurements can be reduced somewhat by very careful adjustment of the coils and great care in the environment of the coils. The value of standard deviation quoted in Section 2.2 is probably good for careful field operation of the coils. Careful laboratory operation could cut the deviation in half.

The vibration testing techniques described in Section 2.3 were quite satisfactory. They appear to have solved, for the type of model tested in this program, the problem of exciting the model without disturbing its mass distribution. Some difficulty can be experienced if two vibration modes have frequencies that are close together. For the wings of this test program this occurred quite frequently for the second bending and first torsional modes, but these modes could be separated adequately by changing the excitation of the wing from primarily force to primarily moment as noted in Section 2.3.

The method of fixing the root of the model for both vibration and flutter test can cause some difficulty if the model vibration frequencies are high. The mount of the model in its support block, as described in Reference 9, was eminently

satisfactory. Care had to be taken, however, in clamping the support block either to a fixed support for vibration tests with the air shaker or to the support plate for vibration tests using the electromagnetic shaker that the clamping arrangement did not introduce spurious vibration modes. Ordinary clamps are unreliable as clamping devices since they seem to have frequencies of about 200 cps which is in the range of natural frequencies for the models. The methods of vibration testing discussed in Section 2.3 neither alleviate nor worsen this problem. It is intrinsic to vibration testing.

It would be desirable to develop a method of obtaining the actual shapes of the natural vibration modes. An optical method was attempted but its accuracy was poor. Miniature accelerometers built into the wing using piezoelectric elements seem to hold the most promise of obtaining accurate vibration mode shapes.

As indicated in Section 2.4, the methods of flutter testing seem satisfactory. No adequate method of determining the complete flutter mode shapes was developed, but it would be desirable to measure them. High speed photography yields a good measure of the model tip motions, but motion of other wing points are difficult to determine from the high speed motion pictures. The most promising method of determining complete flutter mode shapes for classical bending-torsion flutter seems to be miniature accelerometers built into the wing. Accelerometers would have the problem of picking up unwanted noise.

As noted in Section 2.4 shock interference was apparently no real problem for the size of model tested. For certain of the aileron tests, it was suspected that a weak disturbance, existing in the test section and reflecting off the tunnel roof, might be causing aileron buzz. Investigation with a static pressure probe, mounted behind the wing indicated that the shock was very weak. The frequency spectrum of the pressure signal associated with the shock revealed no large component near the aileron buzz frequency. In fact, the static probe recorded very little until after buzz or flutter had started.

It would be desirable, but it is not essential, to keep the density in the tunnel test section constant during a flutter run. Changes in density are important for the lightweight models tested. The flutter tests in this program were all made with density varying in the test section, although the relative density at flutter for most of the models does not vary greatly. The variation in density makes comparison of the flutter data somewhat more complicated, but there are several empirical corrections that work well in correlating flutter data at different relative densities. These are discussed in Reference 2.

In summary, the following conclusion and recommendations are made:

a) In general, the testing techniques and model designs were satisfactory for the testing of supersonic flutter models.

b) For more complete flutter information, vibration and flutter mode shapes should be measured. Miniature accelerometers built into the wing as a part of the wing design seem to offer the most accurate method of determining flutter and vibration mode shapes.

c) It is quite desirable to do flutter testing for low density models at constant air density and a system for controlling density should be developed for the supersonic blow-down tunnel of Reference 9.

REFERENCES

1. Bisplinghoff, R. L., Ashley, H., and Halfman, R. L., Aeroelasticity, Addison-Wesley Publishing Co., Inc., Cambridge, Mass., 1955.

2. McCarthy, et al., Three-Dimensional Supersonic Flutter Model Tests near Mach Number 1.5, Part II, Experimental and Theoretical Results for Bare Wings and Wings with Tip Tanks, Air Force T.R. 54-113 Part II, to be published.

3. Marks, L. S., Mechanical Engineers' Handbook, McGraw-Hill Book Co., Inc., New York, 1951.

4. Timoshenko, S., MacCullough, G. H., Elements of Strength of Materials, D. Van Nostrand Co., Inc., New York, 1940, p83.

5. Schaevitz, H., The Linear Variable Differential Transformer, Society for Experimental Stress Analysis, Volume IV, Number 2, 1947.

6. Davis, H. M., A Method for Measuring Small Deflections, M.I.T. Aeronautical Engineering Department, S. B. Thesis, 1953.

7. Wasserman, L. S., Smilg, B., Application of Three-Dimensional Flutter Theory to Aircraft Structures, Air Force T. R. 4798, July 1942.

8. Prigge, J. S., Jr., The Design of Supersonic Flutter Models, M.I.T., Department of Aeronautical Engineering, A.E. Thesis, August, 1954.

9. Halfman, R.L., McCarthy, J.F., Jr., Prigge, J.S., Jr., Wood, G.A., Jr., A Variable Mach Number Supersonic Test Section for Flutter Research, WADC Technical Report 54-114, December, 1954.

10. Smith, Rodney H., Air Jet Vibrator for Determining Natural Frequencies of Aircraft, M.I.T., Department of Aeronautical Engineering, S.M. Thesis, 1943.

11. Smith, Rodney H., The Aeroelastic Response of a Wing to Harmonic Excitation at Various Airspeeds and Frequencies, M.I.T., Department of Aeronautical Engineering, ScD Thesis, 1948.

12. Halfman, R. L., McCarthy, J. F., Jr., The Design and Testing of Supersonic Flutter Models, Institute of Aeronautical Sciences Paper, to be published.